International Journal of Nanomedicine

Dovepress
Taylor & Francis Group

Open Access Full Text Article

ORIGINAL RESEARCH

Silk Biowaste Protein Mediated Silver Nanoparticles Synthesis and Analysis of Anti-Inflammatory, Wound Healing, Antidiabetic, Antioxidant, Tyrosinase Inhibition, and Antibacterial Mechanism of Action

Gitishree Das[1,2], Han-Seung Shin[2], In-Jun Yang[3], Ly Thi Huong Nguyen[3,4], Jayanta Kumar Patra[1,2]

[1]Research Institute of Integrative Life Sciences, Dongguk University-Seoul, Goyangsi, 10326, Republic of Korea; [2]Department of Food Science & Biotechnology, College of Life Science and Biotechnology, Dongguk University-Seoul, Goyangsi, 10326, Republic of Korea; [3]Department of Physiology, College of Korean Medicine, Dongguk University, Gyeongju, 38066, Republic of Korea; [4]Department of Pathology, University of Alabama at Birmingham, Birmingham, AL, 35294, USA

Correspondence: Jayanta Kumar Patra, Dongguk University-Seoul, Goyangsi, 10326, Republic of Korea, Email jkpatra@dongguk.edu

Background: Silk, a natural biowaste protein from silkworm cocoons called sericin, has promising properties as a biomaterial for several biomedical applications, owing to its excellent biocompatibility, biodegradability, hydrophilicity, and reactivity.

Purpose: The synthesis of AgNPs using these biowaste protein materials is more efficient, environmentally friendly, and cost-effective.

Methods: In this study, a novel approach was developed to synthesize silver nanoparticles (Scn-AgNPs) using sericin as a reducing agent and to study their anti-inflammatory, wound healing, antidiabetic, antioxidant, tyrosinase inhibitory, and antibacterial mechanisms of action.

Results: The initial production of Scn-AgNPs was established by a visual color change to brown, followed by UV-visible spectroscopy, which showed a solid absorption band at 422 nm due to surface plasmon resonance. The mean particle size 82.77 nm with a polydispersity index of 0.387, and −30.8 mV zeta potential specifies the strong stability of the nanoparticles. Scn-AgNPs demonstrated promising wound healing potential, with around 67.72% of wound closure rate at 25 µg/mL concentration. Besides, It also displayed significant anti-inflammatory, antioxidant (in terms of DPPH (75.48%), ABTS (95.04%), SOD (73.92%) potential), antidiabetic properties (95.32% of α-amylase inhibition and 94.42% of α-glucosidase inhibition), and tyrosinase inhibition (27.07%) potentials. Furthermore, the Scn-AgNPs also exhibited significant antibacterial potential with the inhibition zones diameter ranging from 13.84 to 16.90 mm against all the three tested bacteria.

Conclusion: The results indicated that Scn-AgNPs could be a potential candidate for various applications, including cosmetics for preparing antioxidant rich gels and nano formulations, in the biomedical field as a component of wound dressing, antibacterial dressing, drug carriers and drug delivery systems, and in environmental sectors as antibacterial agents, food packaging, food additives and in vitro/in vivo monitoring. This study highlights the use of sericin bio-waste materials into valuable resources, endorsing sustainability and enhancing the commercial value of silk-based bio-waste materials.

Keywords: silk protein, sericin, bio-waste, anti-inflammatory, wound healing, antioxidant, antibacterial mode of action

Introduction

Nanotechnology encompasses the strategy, synthesis, and management of resources that can be appropriately used for necessary applications at the nanoscale level to attain exclusive things.[1,2] Nanocomposites are a unique class of multi-phase nanostructured units. It displays exclusive physiochemical characteristics that make it a possible candidate against

Received: 27 December 2024
Accepted: 7 May 2025
Published: 22 May 2025

several synthetic therapeutic agents.[3] Therefore, they can be used as nanocarriers in drug delivery systems.[4–6] Metallic nanoparticles have established prospective uses, such as embattled antimicrobial applications, drug distribution, cancer treatment, optical devices, catalysis, water treatment electronics, and magnetic fields, because of their unique characteristics.[2,7] Sometimes, metallic nanoparticles, when used alone, can affect biological systems. Thus, to reduce the cytotoxic effect of these metallic nanoparticles and to improve their antimicrobial and other biological effects, it is better to coat them with a biocompatible biological medium.[3] Several reports have suggested the use of nanoformulations and their combinations in biomedical applications.[8–11] In a study by Zhang et al,[12] the author has formulated pH-sensitive, iron-coordinated polymer nanoparticle integrating a mitochondrial-targeting drug for its synergistic tumor therapy.[12] In another study, a nano-biomimetic delivery system was designed that enhances the hypoxia respond to the environment of the cancer cells and was also able to effectively load the photosensitizer indocyanine green helpful in the phototherapy and chemotherapy for cervical cancer treatment.[13]

Nanoparticles manufactured by the organic method are exceedingly good compared to those obtained by chemical and physical approaches because they are inexpensive, environmentally friendly, and are obtained by a one-step procedure.[14] Using a controlled biological approach, nanoparticles of specific sizes and shapes can be produced.[2,7] Recently, noble metals such as silver, gold, and platinum have been extensively investigated for a variety of applications, such as sending, biomedicine, optics, etc.[15] Silver nanoparticles (AgNPs) are well-known nanomaterials owing to their outstanding broad-spectrum biological prospects. Silver nanoparticles (SNPs) have attracted considerable attention owing to their useful properties in the fields of biosensor materials, wastewater treatment, pollution remediation, food packaging materials, composite fibers, etc.[2,16] SNPs can be synthesized using a range of approaches, from the chemical to the physical synthesis process.[17,18] However, recently, researchers have begun using green synthesis methods that are environmentally sustainable, affordable, and non-toxic in nature, without any harmful byproducts.[19,20]

By-products significantly contribute to industrial pollution. Nevertheless, it is likely that these by-products can be converted to valuable substances using suitable management systems.[21] For instance, in the silk/textile industry, water pollution usually occurs when wastewater from the degumming process runs out through drains and mixes with natural water bodies, resulting in high chemical oxygen demand and biological oxygen demand levels in the water bodies.[21] This water pollution is due to the addition of sericin to wastewater.[22] Globally, approximately fifty thousand tons of sericin are abandoned.[23,24] This is an abundant waste of natural resources that causes severe ecological contamination. Hence, the retrieval and recycling of discarded sericin from wastewater bodies could serve two purposes: mitigation of waste-polluted water and utilization in beneficial purposes for economic, social, and environmental advantages. Sericin is a hydrophilic globular protein formed entirely in the silk glands of silkworms. The Cocoons are generally composed of approximately 25% sericin and 75% fibroin, and this 25% sericin protein is thrown away as a waste in the reeling process of silk.[25] Sericin has a number of properties, which make it an excellent component for food packaging and food additive material manufacture. Further, when compared to other proteins and their derivatives, sericin could be explored for biomaterial applications since it has received the FDA approval.[25,26] It possesses many biological properties such as antimicrobial, antioxidant, mitogenic effects promoting cell growth and wound healing potentials.[27–29] Its numerous biological properties promote wound healing and anticancer cell growth, etc.[30–34] Additionally, sericin exhibits a thermoresponsive action comparable to that of gelatin, transitioning between liquid and gel states with temperature changes that could be beneficial for its biomaterial applications in cosmetics, tissue engineering, pharmaceutical, etc. in the wound repair and skin regeneration, as hydrogels, films, conduits, scaffolds etc.[28,33,35–42]

One of the significant property of sericin, ie its unique amino acid composition, aids in its amphipathic and acid-base sensitivity, making it suitable for drug delivery.[43] Latterly, including sericin protein as nano-conjugates has started a promising area of research that influenced the exclusive sericin properties improving the effectiveness and strength of sericin-based nanomaterials. For example, a study by Dan et al[44] have displayed the effective potential of sericin-based nanomaterials in targeted drug delivery and nanocarriers in control release of therapeutic drugs.[44] Combination of sericin with other polymers could enhance its biomedical and pharmaceutical applications, which include regeneration of skin tissue, antibacterial sheets, wound dressing materials, and drug delivery.[45] A number of studies have reported the use of sericin as a reducing and stabilizing agent in the biosynthesis of different types of nanomaterials.[46–48] A report suggests that the shifting of color of the reaction medium and the UV spectral data of the sericin-based nanoparticle proved that

sericin possess a redox potential and is able to reduce the metal ions to synthesize the nanomaterials.[46] Sericin protein contains aspartic acid, and the peptide bond in the aspartic acid is broken when proteins are hydrolyzed by heat during the hydrothermal extraction of sericin, hence it is possible that the aspartic acid in sericin is exposed to the outer part of the protein structure and might act as the reducing agent in the biosynthesis of nanomaterials.[49,50] All these studies not only help in making a proper utilization of sericin biowaste material but also it enhances its commercial value, contributing to a more sustainable application of industrial waste materials. Considering all the potential uses of sericin protein biowaste material, currently, an attempt was made to develop SNPs using sericin as the reducing and stabilizing agent and evaluate its anti-inflammatory, wound healing, antioxidant, antidiabetic, and antibacterial effects in order to explore its major applications in the biomedical, cosmetics and pharmaceutical fields for developing skin care products, antibacterial sheets, wound healing patches and tissue scaffolds etc.

Materials and Methods

Sericin Removal and Synthesis of SNPs

Sericin was removed and purified from silk cocoons (commercially obtained from a local sericulture farm in Gyeonggi-do province, Republic of Korea) using a standard procedure described in our previous publication.[51] The silk cocoon was cleaned properly and dried under room temperature. For extraction of sericin, around 100 gm of finely cut cocoon were boiled with 400 mL of 0.2% of sodium carbonate solution at 121°C for 20 min followed by cooling at room temperature and filtration using Whatman No. 1 filter paper and dialysis for 5 days. After dialysis, the purified sericin was freeze-dried to powder form and stored in airtight vials. Prior to the synthesis, different dilutions (100%–0.78%) of sericin were prepared with warm distilled water and optimized for the manufacture of SNPs. It was found out that 1.5% of sericin solution was ideal for the synthesis of sericin mediated SNPs (Scn-AgNPs); hence, it was used for further large-scale preparation of SNPs. For Scn-AgNP biosynthesis, a previously established procedure was used, with slight modifications.[14,52] Briefly, 180 mL of 1mM $AgNO_3$ salt solution was added to 20 mL of 1.5% sericin solution in a half litre Erlenmeyer flasks and continuously stirred for 24 h at room temperature. The biosynthesis procedure was confirmed by visual changes in the color of the sample solution. After 24 h, the sample was centrifuged (ultracentrifuge, Optima XE-100, Beckman Coulter, USA; 10, 000 rpm for 0.5 h) and washed repeatedly to remove any traces of unattached sericin. Next, the Scn-AgNP pellets were dried in an oven and refrigerated for later use.

Characterization of Bio-Based Sericin Fabricated Scn-AgNPs

Different analytical methods [(UV-VIS spectroscopy, transmission electron microscopy (TEM), energy dispersive X-ray spectroscopy (EDS), atomic force microscopy (AFM), X-ray diffraction (XRD), thermal gravimetric analysis (TGA), zeta potential, particle size, and Fourier-transform infrared spectroscopy (FTIR)] were used to characterize the sericin-fabricated Scn-AgNPs following the standard established protocol of available articles.[53–55] UV-Vis spectra in the range 300–750 nm were measured using a spectrophotometer (Multiskan Go, Thermo Scientific, USA). The size and exterior morphology were investigated using TEM (Tecnai G2 F20/FEI), and the elemental composition was studied using an EDS machine attached to the TEM. Before starting the TEM study, the Scn-AgNPs were diluted, poured onto copper grids, and visualized using TEM. The external nature of the Scn-AgNPs was evaluated using an AFM machine (Bruker Nano Surfaces, USA). Before the AFM measurements, the Scn-AgNP samples were prepared on Si wafer slides. The size distribution and zeta potential of Scn-AgNPs was estimated through DLS (Dynamic Light Scattering) and zeta potential instrument (Malvern Zeta-sizer Nano-ZS, UK) at temperature 25°C. XRD measurements were performed using an XRD machine at a 2θ angle, Cu-Kα radiation at 40 mA, and 30 kV (X'pert MRD; Panalytical Almelo, The Netherlands), and the crystal structure of the Scn-AgNPs was obtained. FT-IR spectral analysis was performed in the 400–4000 cm^{-1} range of transmittance mode (Nicolet iS5 FTIR Spectrometer, Thermo Fisher Scientific, USA). Approximately 2 µL of Scn-AgNP solution was dispensed onto the test sample collection socket, and built-in computer software was used for the analysis. In the Scn-AgNP sample, various types of functional groups were detected when the vibration modes were altered. The thermal stability of bio-based Scn-AgNPs was evaluated using TGA instrument from 25°C to 900°C at 10°C/min ramping time (pyris TGA/N-1000, SNACK, USA).

Biological Prospective of the Bio-Based Scn-AgNPs

The biomedical potential of the bio-based Scn-AgNPs was investigated using a number of standard established assays, such as anti-inflammatory, wound healing, antioxidant, antidiabetic, and tyrosinase inhibition effects, as well as antibacterial activity and antibacterial mode of action.

Anti-Inflammatory Effect of Scn-AgNPs

For cell viability and enzyme-linked immunosorbent tests of Scn-AgNPs, a previously described procedure was followed, the details of which are provided.[51,56] The RAW264.7 cells from the cell line bank (in Seoul, Korea) were used in the study. The transmission density of the reaction mixture was determined at 570 nm for the cell viability assay and at 450 nm for the ELISA assay (using ELISA kits, Koma Biotech Inc., Republic of Korea).

Wound Healing

HaCaT cells (immortalized cell line) provided by the Korea Institute of Oriental Medicine (Daegu, Korea), were used for the wound healing assay, and both cell viability and scratch wound assays were performed as per the regular processes discussed in detail in our previous study.[51] *Centella asiatica* extract (100 µg/mL; United States Pharmacopeia Reference Standard, Sigma Aldrich) was used as the positive control and Scn-AgNP samples at various concentrations (5, 10, and 25 µg/mL) were used as treatment samples. Finally, the scratch gap width images were taken using an automated imaging system (Lionheart FX) at consistent time breaks, and the measurements were performed using Gen5 Imager software (Biotek Instruments Inc., USA).

The wound closing rate was assessed as mentioned below:

$$\text{Wound closing}(\%) = \frac{(\text{ORSGW} - \text{OPSGW})}{\text{ORSGW}} \times 100$$

where ORSGW is the width of the original scratch gap and OPSGW is the width of the open scratch gap on one complete day.

The Scn-AgNPs Antioxidant Assay

The antioxidant potential of Scn-AgNPs was evaluated using four types of antioxidant tests: DPPH (1,1-Diphenyl-2-picrylhydrazyl) free-radical scavenging, ABTS (2,2-Azinobis-3-ethylbenzothiazoline-6-sulfonic acid) free-radical scavenging, superoxide dismutase (SOD) inhibition, and reducing power tests by the regular technique as defined earlier.[55,57] Furthermore, the effective concentrations displaying 50% effect has also been calculated and recorded as the EC_{50} or the $EC_{0.5}$ values. For the DPPH assay, different concentrations of Scn-AgNPs (25, 50, and 100 µg/mL) and ascorbic acid (ASA) as the positive controls. The transmission density of the reaction solution was obtained using a UV-VIS multiwell plate reader at 517 nm (Multiskan Go; Thermo Scientific, USA) and the outcomes were estimated using the following equation:

$$\text{Percentage scavenging} = \frac{\text{Control}_{\text{readings}} - \text{Test}_{\text{readings}}}{\text{Control}_{\text{readings}}} \times 100 \ldots\ldots\ldots \text{equation(A)}$$

Here, $\text{Control}_{\text{readings}}$ is the transmission density of the control and $\text{Test}_{\text{readings}}$ is the transmission density of the treatment (Scn-AgNPs/positive control).

For the ABTS scavenging effect of Scn-AgNPs, 30 µL of Scn-AgNPs and the standard ASA were added to the phial containing ABTS solution (270 µL) and set aside in the dark (120 min). Their transmission density was measured at 734 nm, and the ABTS free radical scavenging percentage was calculated using equation A. The SOD inhibition effect of Scn-AgNPs was estimated using the Oxiselect superoxide dismutase assay kit and procedure (MyBioScource.com).[55] The percentage of SOD inhibition was determined as 490 nm using Equation (A). Butylated hydroxytoluene (BHT) was used as positive control. The reducing power of Scn-AgNPs was evaluated as previously described. Finally, the transmission density of the reaction mixture was obtained at a wavelength of 700 nm, and the outcome was displayed as the transmission density value.

The Scn-AgNPs Antidiabetic Prospective

The antidiabetic potential of Scn-AgNPs was estimated using α-amylase and α-glucosidase inhibition assays following well-established protocols with minimal modifications.[58] For the α-amylase assay, Scn-AgNP/acarbose (25–100 µg/mL), phosphate buffer (pH 6.9) (20mM), and α-amylase (4 U/mL) were mixed together (200 µL) and incubated for 5 min. Initiation of the reaction process was initiated by the addition of 0.5% potato starch (200 µL) and further incubation for 3 min. Next, 3,5-dinitro salicylic acid reagent (200 µL) was mixed and boiled at 85–90°C in water bath for 10 min to develop color. Then after cooling, the transmission density values were obtained at 540 nm (by UV-VIS multiwell plate reader; Multiskan GO; Thermo Scientific, USA), and the percentage activity was computed using Equation A. For α-glucosidase assay, in short, Scn-AgNPs/acarbose (25–100 µg/mL), potassium phosphate buffer (pH 6.8) (67 mM), α-glucosidase (4 U/mL) were mixed together (1000 µL) and incubated for 10 min at 37°C. The assay was initiated by the addition of 3 mM p-nitrophenyl-α-d-glucopyranoside (100 µL) and incubating for 20 min at 37°C. The process was terminated by adding a 0.1 M sodium carbonate solution (2000 µL), and then collecting the transmission density values at 405 nm (by UV-VIS multiwell plate reader; Multiskan Go; Thermo Scientific, USA). α-Glucosidase activity was measured using Equation A.

The Scn-AgNPs Tyrosinase Inhibition Assay

The effect of Scn-AgNPs on tyrosinase inhibition was evaluated using a standard method.[55] Briefly, Scn-AgNPs/Kojic acid (25–100 µg/mL), phosphate buffer (pH 6.5) (0.1 mM), mushroom tyrosinase (50 U/mL), and L-DOPA (0.1 mM) were mixed together to make a 300 µL solution and kept at normal temperature for ½ h. The transmission density was measured at 475 nm (by UV-VIS multiwell plate reader; Multiskan Go; Thermo Scientific, USA) and tyrosinase resistance was estimated using Equation A.

The Scn-AgNPs Antibacterial Action and Mechanism Studies

Three foodborne pathogenic bacteria (pathogenic) like *Escherichia coli* O157:H7 (ATCC 23514), *Enterococcus faecium* (DB01), and *Listeria monocytogenes* were selected for antibacterial evaluation and determination of the antibacterial mechanism of action. The foodborne pathogenic bacteria were obtained from the microbiology laboratory of our department. All bacterial cultures were maintained in slant culture and subcultured in nutrient broth medium prior to use.

The Scn-AgNPs Antibacterial Screening

A standard disc diffusion assay was referred.[55] Ciprofloxacin (10 µg/paperdisc) was used as the positive control and Scn-AgNPs (100 µg/paper disc) were used as the test samples. Prior to the test, nutrient agar plates were evenly seeded with the test pathogens (10 µL), followed by placing the paper disc at strategic points, and for overnight at 37°C in a bacteriological incubator (SL-64, 150, HYSC limited, Republic of Korea). The final result was recorded as the diameter of the zone of inhibition (dZOI) formed over the tested discs (mm). Minimum inhibitory concentration (MIC) and minimum bactericidal concentration (MBC) were evaluated using standard procedures.[59] The minimum concentration of test sample, which showed no visible growth of the pathogen was selected as the MIC and the lowest concentration of test sample, where no growth of the pathogen was seen in the nutrient agar plate was selected as the MBC. To study the mechanism of antibacterial action, three assays, including bacterial cell viability, loss of salt tolerance, and the effect on 260 nm absorbing materials were performed using two pathogenic bacteria, *E. coli* and *E. faecium*.

The bacterial cell viability assay was performed by time-kill test using the normal technique defined earlier.[55] For this assay, the two pathogenic bacterial cultures were used as the control group and the bacterial cultures treated with Scn-AgNPs at MIC were used as the treatment. Briefly, 10 mL of pathogenic culture comprising 10^7 CFU/mL was used for both the control and the test vials and incubated at 37°C. The culture was collected at regular time intervals, serially diluted, applied to agar plates, and incubated for 1 d. The bacterial colonies grown on the control and treated plates were counted and recorded as log CFU/mL.

The tolerance efficacy of the two tested bacteria treated with Scn-AgNPs at MIC to the concentration of salt was scrutinized using an established standard technique.[55] Full-grown bacterial cultures with Scn-AgNPs treatment at MIC and same number of cultures without any treatment were used as controls and incubated at 37°C for 60 min. Further, the samples

were serially diluted and sown on nutrient agar (NA) test plates with (0%, 2.5%, 5.0%, and 10.0%) of salt. Subsequently, the number of bacterial colonies grown on the control and treated plates were counted and recorded as log CFU/mL.

The effect of the Scn-AgNPs on the bacterial cell membrane was investigated using a 260 nm absorbing material assay.[55] The Scn-AgNPs (MIC concentration) were added to the bacterial culture (2000 µL) in peptone water (100 mg/100 mL) and incubated at 37°C. The bacterial test samples were collected at regular time intervals and centrifuged (at 1.5 K rpm, 10 min), and the transmission density value of the supernatant was determined for the presence of DNA and RNA (cellular materials) released into the extracellular matrix at 260 nm. For this experiment, peptone water (merely) with Scn-AgNPs at MIC was used as the control (negative) and peptone water with pathogenic bacteria cultures was used as the positive control.

Statistical Analysis of Scn-AgNPs

All experiments were performed three times, and the resulting data are denoted as the average values of three autonomous results with standard deviations. Further, ANOVA and Duncan's multiple range tests, at 5% level of significance. $P < 0.05$ was also performed with SPSS version 27.0 (IBM Corp., Armonk, NY, USA).

Results and Discussion

In this study, sericin protein was removed from *Bombyx mori* L. silk cocoons by degumming and purified through dialysis. Purified sericin was used as the reducing agent for the biosynthesis of Scn-AgNPs (Figure 1A). For the biofabrication of Scn-AgNPs, various dilutions of sericin (100%–0.78%) tested initially for reducing agent. Finally, 1.56% sericin concentration was used for AgNP synthesis. Report suggested that there is no major role of temperature variation in the synthesis process of sericin-based nanoparticles, however nanoparticles performed well at higher pH,[34] hence in the current study, an alkaline pH condition was used for extraction of sericin, and subsequently this sericin material was used for synthesis of Scn-AgNPs. In the biosynthesis process, the mixture containing the Scn-extract and $AgNO_3$ solution was initially colorless, and after 12 h, the color gradually turned light brown and brown after 24 h (Figure 1A). The sample was kept for two month for checking its stability and it was found that there was no change in its physical nature after two months, which proves that the sample is physically stable *Bombyx mori* silk sericin comprises 18 amino acids, primarily serine, tyrosine, glycine, glutamic acid, valine, and threonine residues, among which tyrosine displays robust electron-donating properties and can aid in reducing the Ag^+ ions to form Ag^0 atoms, which then aggregate to form silver nanoparticles.[14,24] Previously studied report suggested that sericin possess a redox potential and is able to reduce the metal ions to synthesize the nanomaterials.[46] Another study suggested that, sericin protein contains aspartic acid, and the peptide bond in the aspartic acid is broken when proteins are hydrolyzed by heat during the hydrothermal extraction of sericin, hence it is possible that the aspartic acid in sericin is exposed to the outer part of the protein structure and might act as the reducing agent in the biosynthesis of nanomaterials.[49,50]

Following visual confirmation, UV-visible absorption spectra were also recorded, which displayed a solid absorption band in the noticeable region at 422 nm owing to surface plasmon resonance, confirming the synthesis of Scn-AgNPs (Figure 1A). Similarly, results on SNPs are also established from earlier stated reports.[14,60–62] The Scn-AgNPs demonstrated a single absorption peak at 422 nm, which reinforced the spherical shape of the synthesized nanoparticles along with their chemical stability, in agreement with the TEM results discussed subsequently (Figure 1B).

Further characterization of the synthesized Scn-AgNPs was done by a number of standard procedures. TEM is considered an excellent tool for gathering data on the morphology and size of the produced NPs.[63] The TEM images of Scn-AgNPs (Figure 1B and C) show the morphological features of the Scn-AgNPs. The mean diameter of the oval-spherical shaped Scn-AgNPs was found to be 8.33 nm. The TEM micrographs indicated that the round-shaped Scn-AgNPs had planar edges. In addition, to check the crystalline characteristics of the produced Scn-AgNPs, TEM analysis was performed after 4 months of complete synthesis of Scn-AgNPs; however, the NPs did not agglomerate, which established the stability of the Scn-AgNPs. Selected-area electron diffraction (SAED) patterns were recorded (Figure 1C). The SAED pattern with bright circular spots indicated that the Scn-AgNPs were crystalline in nature. The elemental arrangement of the synthesized Scn-AgNPs was determined by EDS analysis, which revealed a maximum percentage of silver with minor signal peaks, such as Mg, Fe, O, and Si, in the nanoparticle mixture (Figure 1D). AFM analysis was performed to detect the morphology of Scn-AgNPs in 2D and 3D (Figure 1E and

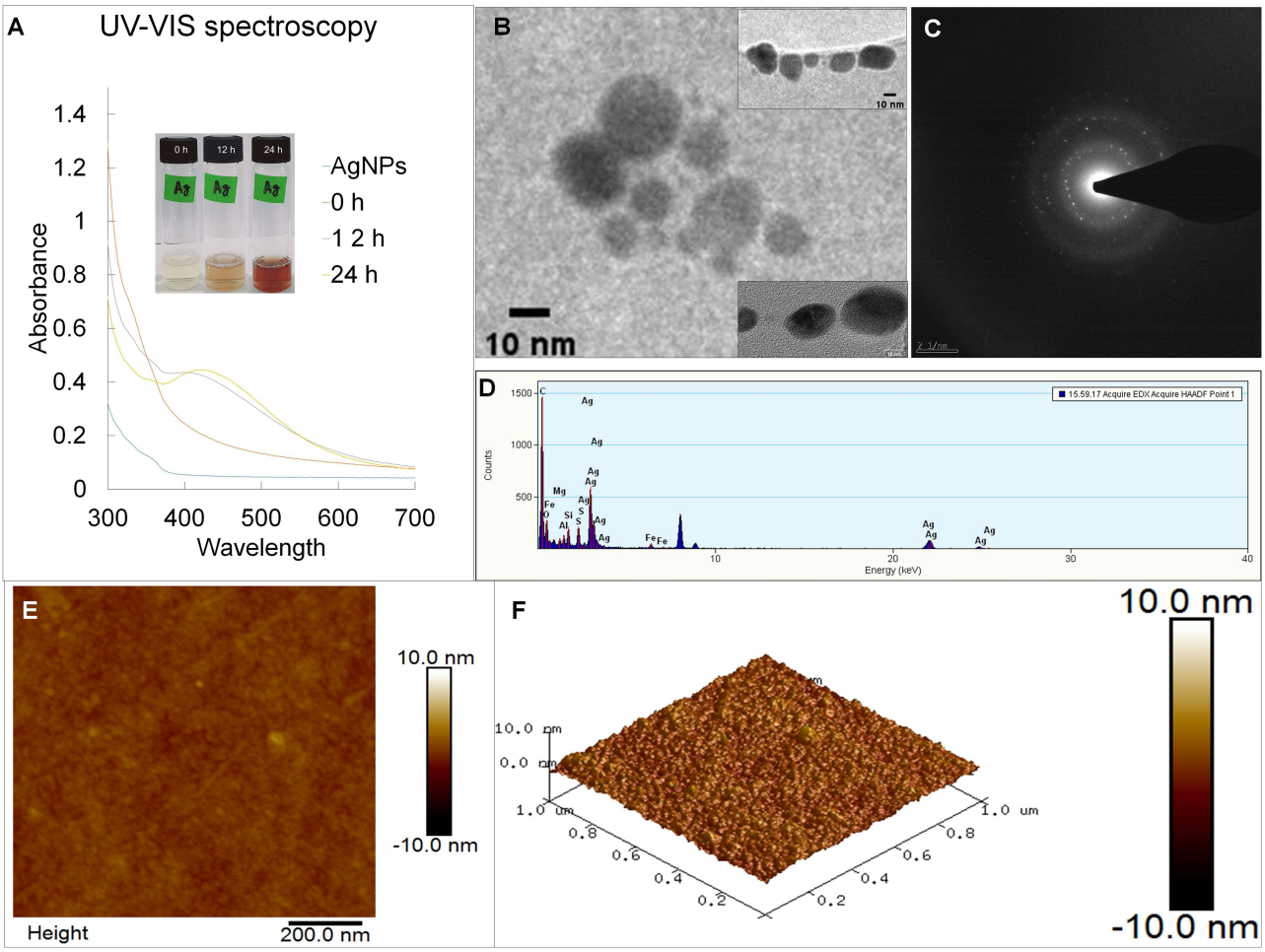

Figure 1 Characterization of Scn-AgNPs. (**A**) UV-VIS spectroscopy with color change at time intervals; (**B**) Transmission electron microscopy image (inset: magnified view); (**C**) Selected area electron diffraction pattern (SAED) images (**D**): Energy-dispersive X-ray spectroscopy image; (**E**) 2D Atomic force microscopy image; (**F**) 3D Atomic force microscopy image.

F). The results showed clear and distinct spherical nanoparticles in the range–1–10 nm. The 3-D image of Scn-AgNPs shows sphere-shaped crystalline and grain nanoparticles. This result is consistent with those of previously published studies.[64,65]

The crystalline nature of the Scn-AgNPs was examined using XRD (Figure 2A). The graph displayed several peaks observed at 2θ = 38.14°, 46.31°, 64.67 °, and 78.48°, which are assigned to the (111), (200), (220), and (311) Bragg planes, respectively (Figure 2A). These planes endorse the Scn-AgNPs, signifying a face-centered cubic (FCC) crystal structure matched to pure silver (JCPDS file No.00004–0783).[14,24] The most noteworthy peak at 38.14° indicates that the (111) plane is the foremost constituent of the silver planes. This outcome also confirms the observation of the TEM images in Figure 1B and C, which suggests that the synthesized Scn-AgNPs are crystalline in nature.[66] The mean crystalline size of the synthesized Scn-AgNPs was obtained as 32.07 nm from the XRD pattern using Scherrer's equation and a degree of crystallinity was measured as 67.94% using the OriginPro 2024, version 10.1.[67] These results are similar to earlier reported research outcomes.[68,69]

The effect of high temperature on the Scn-AgNPs was investigated by TGA, and the results are presented in Figure 2B. The results showed that the degradation of Scn-AgNPs due to high temperature was attained in three phases with an overall weight loss of 81.93% (Figure 2B). In the first phase, a weight loss of 16.26% was attained at 285°C, which was attributed to the attached H_2O and other minor molecules to the surface of nanoparticles. In the 2nd phase, a weight loss of 38.50% was obtained between 285°C and 775°C, which was due to the loss of biological materials. As

https://doi.org/10.2147/IJN.S512524

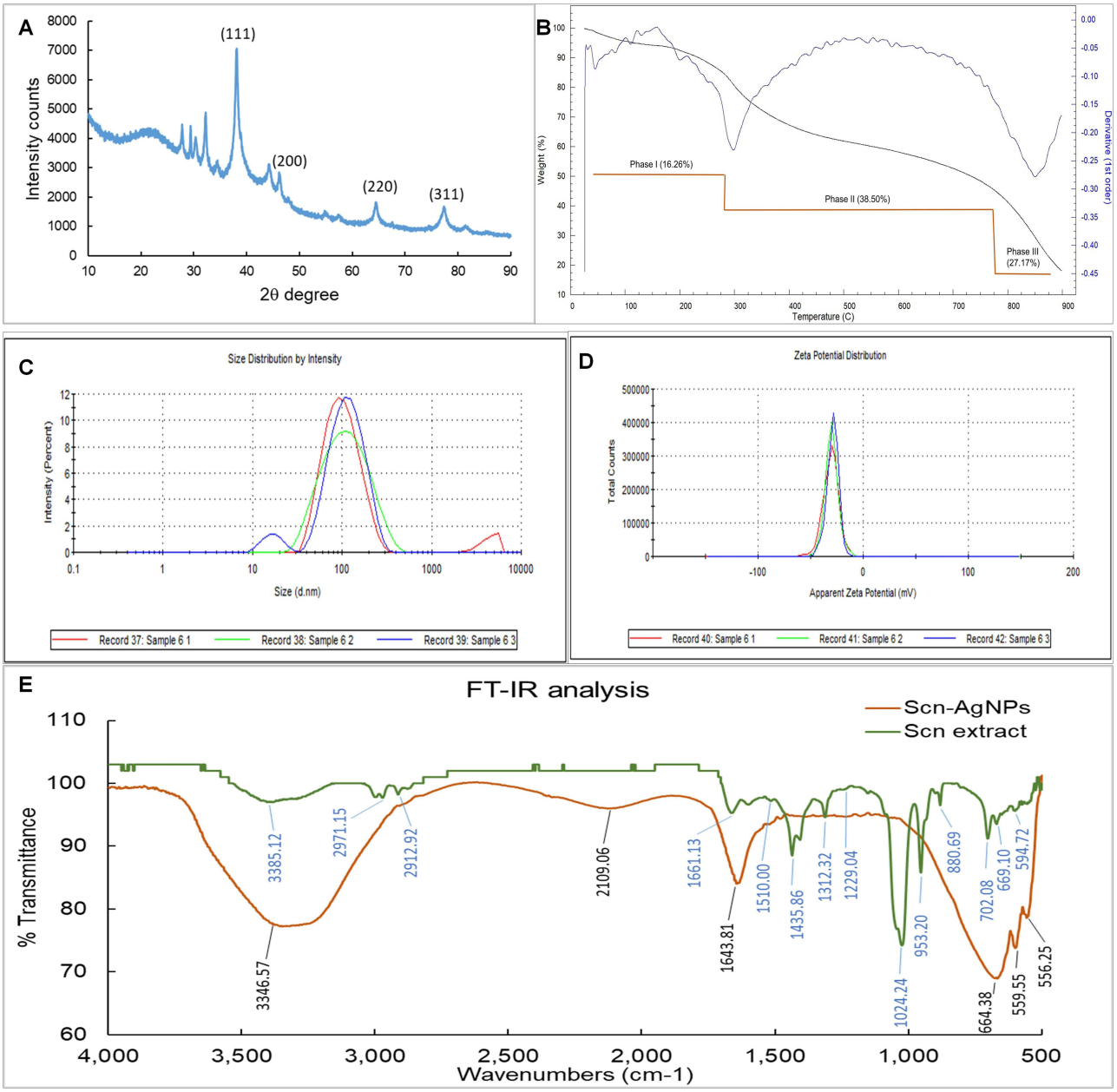

Figure 2 Characterization of Scn-AgNPs. (**A**) X-ray diffraction spectroscopy of Scn-AgNPs; (**B**) Thermogravimetric analysis image; (**C**) Particle size distribution of Scn-AgNPs and; (**D**) Zeta potential of Scn-AgNPs, (**E**) Fourier-transform infrared spectroscopy Scn extract and Scn-AgNPs.

the heat further increased, a 3rd phase was attained between 775°C and 900°C, amounting to nearly 27.17% of weight loss (Figure 2B), which could be due to the loss of the remaining compounds existing in the tested sample. The highest weight loss in the 2nd phase could be attributed to the amplified number of intermolecular interactions for each Scn-AgNP molecule with an increase in Scn concentration.[70,71]

A particle size analyzer and Zetasizer DLS instrument were used to obtain the hydrodynamic size, surface charge, and zeta potential of the Scn-AgNPs under ideal synthesis and operating conditions. The mean particle size was found out as 82.77 nm (polydispersity index (PDI) = 0.387) (Figure 2C). The size of the Scn-AgNPs calculated from the particle size analyzer was larger than that calculated from TEM (Figure 1B and C), which could be due to the impact of Brownian motion.[14] The zeta potential of the Scn-AgNPs was found to be −30.8 mV, indicating the strong stability of the nanoparticles (Figure 2D). Negative zeta potential measurements indicated the exterior charge of the Scn-AgNPs. The

greater zeta potential indicates the enormous electrical charge on the Scn-AgNP surface, resulting in a robust repulsive force between the NPs and is responsible for the greater stability and superior colloidal quality of the synthesized nanoparticles.[72–74] Similar results have been reported similar results.[75–77]

FT-IR analysis was performed to detect the main functional groups present in the Scn extract and Scn-AgNPs and to illustrate the nature and properties of the synthesized nanoparticles. As shown in Figure 2E, the FTIR spectra of Scn-AgNPs and Scn from 4000 to 500 cm^{-1} showed prominent bands. Approximately 14 bands were identified in the Scn extract, whereas, only six bands were identified in the Scn-AgNP spectra. The FTIR spectrum of Scn extract displayed 3385.12 cm^{-1}, 2971.15 cm^{-1}, 2912.92 cm^{-1}, 1661.13 cm^{-1}, 1510.00 cm^{-1}, 1435.86 cm^{-1}, 1312.32 cm^{-1}, 1229.04 cm^{-1}, 1024.24 cm^{-1}, 953.20 cm^{-1}, 880.69 cm^{-1}, 702.08 cm^{-1}, 669.10 cm^{-1}, and 594.72 cm^{-1} distinctive peaks (Figure 2E). While in Scn-AgNPs, the FTIR spectrums displayed 3346.57 cm^{-1}, 2109.06 cm^{-1}, 1643.81 cm^{-1}, 664.38 cm^{-1}, 559.55 cm^{-1} and 556.25 cm^{-1} peaks (Figure 2E). In the FT-IR spectra of Scn-AgNPs, the major peaks of pure sericin were preserved, indicating the active topping of sericin on Scn-AgNPs. A deviation in the peak values was observed between Scn and Scn-AgNPs, which might be attributed to the altered stretching modes between the peaks (Figure 2E). In the case of the Scn-AgNPs, the peak at 3346.51 cm^{-1} could be attributed to the N-H stretch of the 1° and 2° °amines or the O-H stretching of alcohols and phenol functional groups. At 1643.81 cm^{-1}, indicating the existence of a–C=C– stretch bond (medium) of the alkene or the N-H bend of 1° °amines. At 559.55 cm^{-1} and 556.25 cm^{-1}, the peaks indicates the presence of alkyl halides. The absence of FT-IR bands between 3300 and 2400 cm^{-1} indicates the precipitation of protein, and these FT-IR results suggest that protein nanoparticle interactions might have occurred due to the free amine groups and electrostatic interaction of carboxyl groups, as proposed in an earlier study.[78] In case of the Scn extract, the detected peak at 1661.13 cm^{-1}, 1510.00 cm^{-1}, 1229.04 cm^{-1}, belongs to the characteristic absorption bands in sericin protein like amide I (1600–1700 cm^{-1}), II (1504–1582 cm^{-1}), and III (1200–1300 cm^{-1}), respectively.[79] The peak at 1229.04 cm^{-1} might be attributed to the phenolic hydroxyl group of the tyrosine residues of sericin, and the disappearance of this peak in the case of the Scn-AgNPs is probably due to the oxidation of the phenolic hydroxyl group by the silver ion.[24] Furthermore, a carboxyl group peak was recognized at 1435.86 cm^{-1} in the FTIR spectrum of the Scn extract (Figure 2E), which was supposed to support the anisotropic growth of the NPs to nanoplates.[80] These results confirmed the synthesis of Scn-AgNPs, which is in good agreement with former studies.[79,81,82]

The biological potential of Scn-AgNPs was explored using anti-inflammatory, wound healing, antioxidant, antidiabetic, tyrosinase inhibition, antibacterial, and mechanistic studies.

In case of the anti-inflammatory effects, it was initially observed that although the cell viability declined at the concentrations of 10 and 25 µg/mL, but, it was around 80% at 10 µg/mL, and hence the Scn-AgNP toxicity was not very high (Figure 3A). Usually, pro-inflammatory cytokines such as IL-6, IL-1β, and TNF-α play a major role.[83] The Scn-AgNPs repressed the building of pro-inflammatory cytokine (IL-6) augmented by lipopolysaccharide (LPS) treatment, so it was judged to have a positive anti-inflammatory effect (Figure 3B–D). Previous studies have demonstrated the anti-inflammatory potential of sericin protein,[84,85] which was also demonstrated in the current study.

The Scn-AgNPs wound-healing effect of Scn-AgNPs was evaluated using a scratch wound test. The wound healing effects are shown in Figure 4. Similar to the previous experiment, in this case also, Scn-AgNPs were referred to cell viability test (toxicity test), and the results indicated that, in all the three tested concentrations, the cell variability was more than 80% (Figure 4A), indicating negligible toxicity of Scn-AgNPs at these concentrations. The wound closure rate was determined after ½ day and 1 day of incubation, and the corresponding wound was visualized using a scratch wound assay (Figure 4B and C). After 24 h of exposure, the rates of wound closure was found out as 64.17%, 67.17%, and 67.72% at three different concentrations of Scn-AgNPs (5 µg/mL, 10 µg/mL, and 25 µg/mL) correspondingly, compared to the control sample (55.01%) and *Centella asiatica* (positive control) showing 71.02%) (Figure 4B and C). Scn-AgNPs displayed positive wound-healing effects; however, their percentage pattern was not the same as anticipated. Wound healing is a multifarious phenomenon that occurs because of damage to organ arrangements or skin tissues. Cell injury involves the reformation of injured tissues and the specific control of angiogenesis, re-epithelialization, and connective tissue repair.[86,87] SNPs enhance tissue repair, angiogenesis, wound closure, re-epithelialization, and collagen deposition in mice.[88] Keratinocytes play a vital role in the wound healing process, mainly during the proliferation period, and consist of reepithelialization and tissue granulation.[89,90] Keratinocytes are the regular epidermal cells of the skin.[89] The

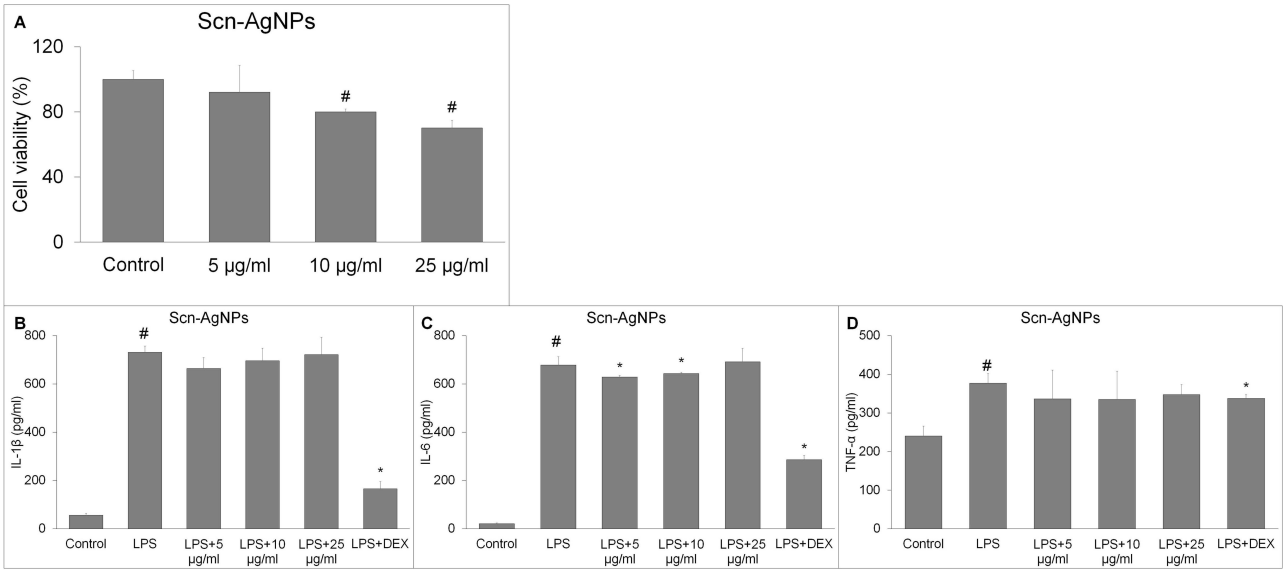

Figure 3 Anti-inflammatory potential of Scn-AgNPs. (**A**) Cell viability assay; (**B**–**D**): MTT assay. #P < 0.05 vs Control, *P < 0.05 vs LPS.
Abbreviations: LPS, lipopolysaccharide; DEX, dexamethasone.

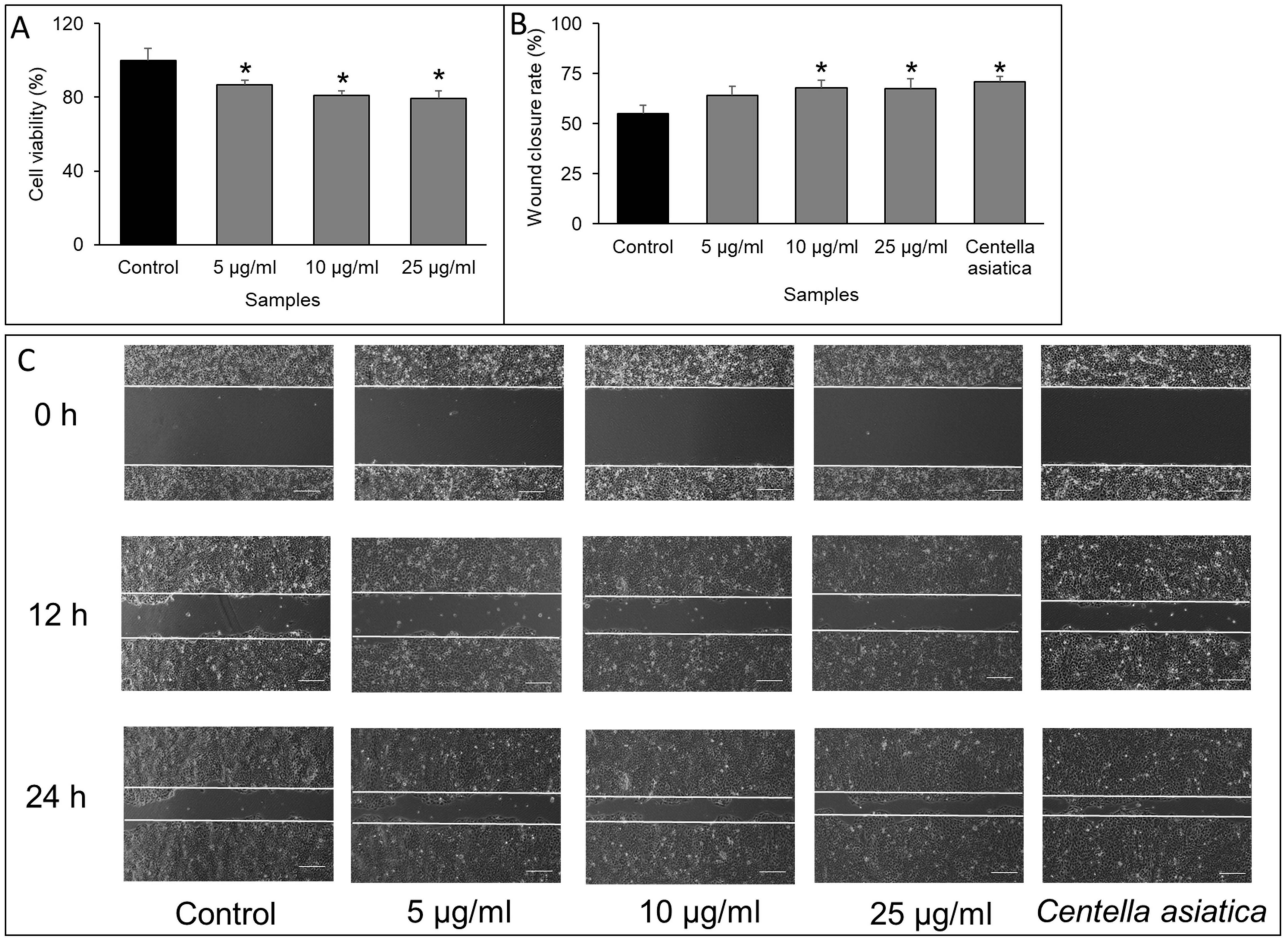

Figure 4 Wound healing effect of Scn-AgNPs. (**A**): Viability of cell count; (**B**): Wound closure rate of Scn-AgNPs; (**C**) Scratch wound test pictures after incubation (at 0, 12, and 24 h). * P< 0.05 vs Control. Scale: 250 µm.

binary mechanisms contributing to wound healing include increased keratinocyte proliferation and migration. In the current case, the efficiency of Scn-AgNPs in wound healing was probably due to their increased movement, as evidenced by the cell viability assessment. Another study showed that the sericin amino acid present in sericin, contributes to early adhesion of the cells and promotes the fibroblast wound healing, thus the wound healing potential of the sericin-based silver nanoparticle (Scn-AgNPs), can be attributed to this concept effect.[91]

Furthermore, the antioxidant potential of Scn-AgNPs was evaluated using DPPH, SOD, ABTS, and reducing power analyses (Figure 5). Bio-fabricated Scn-AgNPs displayed 75.48% of DPPH scavenging potential at 100 µg/mL, as matched to 78.13% scavenging by ASA at the same concentration (Figure 5A). Similarly, the Scn-AgNPs showed an increase ABTS scavenging potential at 25, 50, 100 µg/mL concentrations, with a maximum of 95.04% scavenging, matched to 92.51% by ASA at 100 µg/mL (Figure 5B). In case of SOD assay, the Scn-AgNPs showed a higher inhibition percentage of 73.92% than the used standard positive control BHT, which displayed 61.28% at 100 µg/mL (Figure 5C). Additionally, Scn-AgNPs exhibited an escalating reducing power with a maximum activity of 0.1202, matched to 0.8434 by the standard ASA at 100 µg/mL (Figure 5D).

Additionally, the EC_{50}/ $EC_{0.5}$ values of Scn-AgNPs and reference positive controls were calculated (Table 1). The EC_{50} values of Scn-AgNPs for all the antioxidant parameters are DPPH (54.28 µg/mL), ABTS (34.53 µg/mL), SOD (41.91 µg/mL) (Table 1). For the reducing power, the $EC_{0.5}$ value is 322.70 µg/mL (Table 1). Correspondingly, the EC_{50} and the $EC_{0.5}$ values for reference positive controls were calculated as 37.52 µg/mL (ASA), 31.60 µg/mL (ASA), 48.73 µg/mL (BHT) and 50.93 µg/mL (ASA) for DPPH, ABTS, SOD and reducing power tests correspondingly (Table 1). In conclusion, Scn-AgNPs exhibited significant antioxidant effects in all four assays. A few reports have suggested that the antioxidant potential of sericin could be attributed to the presence of higher amounts of amino acids with hydroxyl groups, such as serine, which act as metal chelators.[32,92] Several studies on the antioxidant potential of sericin have reported earlier.[32,92–94] Another property of sericin is its promotion of cell proliferation. Sericin protein contains carboxyl, amino and hydroxyl groups in more amount, which are able to scavenge the free radicals and decrease

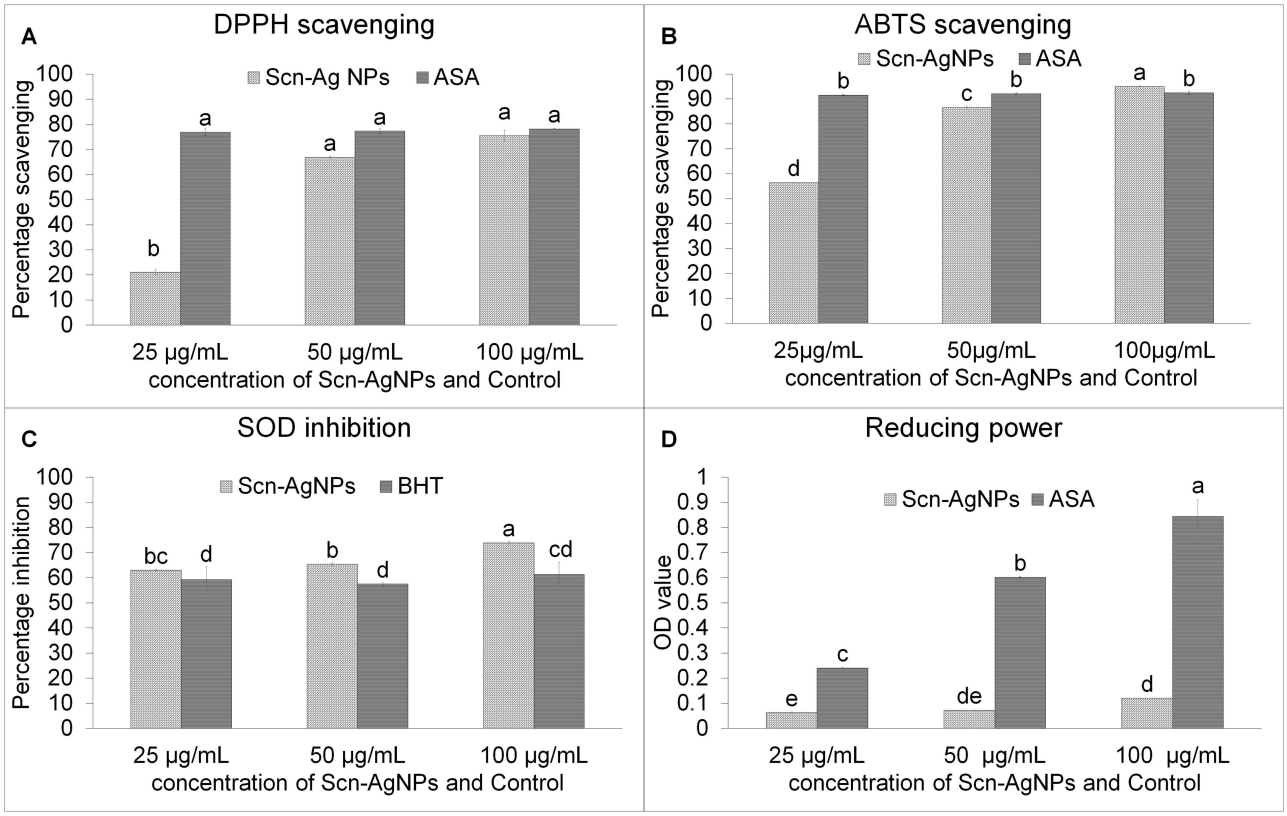

Figure 5 Antioxidant potential of Scn-AgNPs. (**A**) DPPH scavenging study; (**B**) ABTS scavenging study; (**C**) SOD inhibition assay; (**D**) Reducing power study. Difference in the superscript letters are statistically significant at P< 0.05.

https://doi.org/10.2147/IJN.S512524

Table 1 EC_{50} and $EC_{0.5}$ of Different Parameters of Scn-AgNPs and the Reference Positive Controls

Parameters	Scn-AgNPs (in µg/mL)	Reference Positive Controls (in µg/mL)
DPPH scavenging	54.28	37.52 (ASA)
ABTS scavenging	34.53	31.60 (ASA)
SOD inhibition	41.91	48.73 (BHT)
Reducing power ($EC_{0.5}$)	322.70	50.93 (ASA)
α-amylase inhibition	38.51	51.37 (Acarbose)
α-glucosidase inhibition	15.19	416.67 (Acarbose)
Tyrosinase inhibition	135.94	95.73 (Kojic acid)

the effect of oxidative stress in the cell, thus protecting the cell membrane rendering antioxidant effects.[95–97] Besides, a report suggested that application of sericin protein was able to inhibit the epidermal oxidative stress, thereby displaying photopreventive effects against UVB-induced acute damage and tumor promotion in the skin of hairless mouse.[22] Considering this, it can be concluded that the enhanced antioxidant potential of Scn-AgNPs can be ascribed to the effect of the sericin protein, which acts as a reducing, stabilizing, and capping agent in the formulation of Scn-AgNPs. Bioactive compounds present in the sericin extract, along with the silver ions in the Scn-AgNPs, might have served as antioxidants by the transfer of a single electron and hydrogen atom.[98–101]

The antidiabetic potential of Scn-AgNPs was assessed by α-amylase and α-glucosidase inhibition experiments, and the results are shown in Figure 6. Figure 6A shows a clear trend of increased α-amylase inhibition with increasing α-amylase concentration. Maximum inhibition activity of 95.32% by Scn-AgNPs was observed at 100 µg/mL, which was related to the 61.81% exhibited by the acarbose (positive control) (Figure 6A). Furthermore, in case of the α-glucosidase inhibition experiment high inhibition activity of 94.42% was exhibited by the Scn-AgNPs at 100 µg/mL was related to only 1.05% exhibited by the acarbose (positive control) (Figure 6B). The EC_{50} values for Scn-AgNPs was calculated as 38.51 µg/mL and 15.19 µg/mL for both α-amylase and α-glucosidase inhibition assays as related to 51.37 µg/mL and 416.67 µg/mL for acarbose for the same assays (Table 1). These data clearly demonstrate that a small amount of Scn-AgNPs is highly effective against both enzymes, whereas a much higher concentration of acarbose is required to obtain the same inhibitory effect. It has been reported that both α-amylase and α-glucosidase are key to hyperglycemia, and their minimization in the body will help in the fight against diabetes.[102] Usually, α-amylase is responsible for transmuting composite starch molecules into their lower form of glucose; thus, if enzyme activity is restricted, it will help in controlling the body's carbohydrate metabolism, consequently decreasing the absorbed glucose quantity.[103,104] Another important tactic for the interruption of a vociferous upsurge in the blood sugar level in the body is to avert the starch-blocking enzyme (α-glucosidase) effect.[103] Hence, the effective inhibition of both enzymes by Scn-AgNPs could aid in the application of modern antidiabetic drugs or drug carriers. Earlier studies have shown that when sericin protein was administered orally to type 2 diabetic mice, it considerably reduced the blood glucose level (under fasting), plasma insulin (under fasting), and glycosylated serum protein levels, followed by enhanced oral glucose and insulin tolerance, and improved antioxidative activities,[105] which proves the antidiabetic potential of sericin. Similarly, in another study, oral sericin administration in streptozocin-induced type 2 diabetes rats clearly confirmed the hypoglycemic effects primarily associated with decreased oxidative stress in the damaged liver and pancreas of type 2 diabetes rats.[106] Hence, the effective antidiabetic potential of Scn-AgNPs observed in the current study (Figure 6) could be attributed to the sericin-mediated synthesis of Scn-AgNPs.

Tyrosinase inhibition revealed a moderate positive activity of Scn-AgNPs against tyrosinase (Figure 6C). Maximum activity of 27.07% was exhibited by the Scn-AgNPs, matched to 52.23% by kojic acid (positive control) (Figure 6C). The EC_{50} values for Scn-AgNPs and Kojic acid are computed as 135.94 µg/mL and 95.73 µg/mL correspondingly (Table 1).

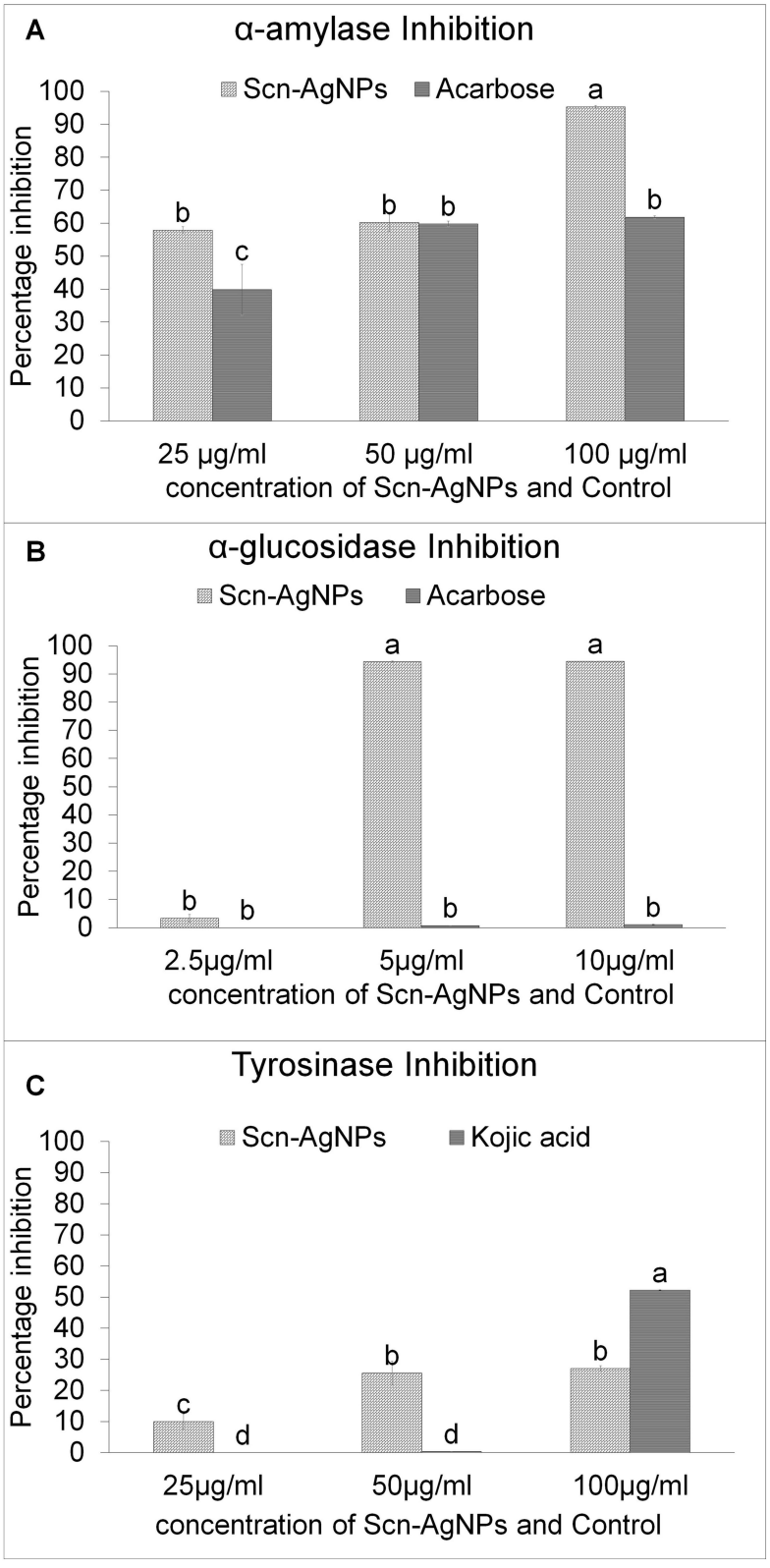

Figure 6 Antidiabetic and tyrosinase inhibition potential of Scn-AgNPs. (**A**) α-amylase inhibition study; (**B**) α-glucosidase inhibition study; (**C**) tyrosinase inhibition study. Difference in the superscript letters are statistically significant at $P< 0.05$.

https://doi.org/10.2147/IJN.S512524

However, the effect of Scn-AgNPs was less than that of kojic acid, but showed a positive trend that increased with increasing sample concentration (Figure 6C). Few reports have demonstrated the antityrosinase effect of sericin protein,[107–109] and this could be attributed to the positive antityrosinase effect displayed by Scn-AgNPs synthesized using sericin protein. Melanin is a skin pigment formed by melanocyte cells in the stratum basale.[110] They are produced to protect the skin from the harmful effects of ultraviolet rays; however, excessive production and accumulation of melanin in the skin often give rise to innumerable skin diseases, such as age spots, hyperpigmentation, solar lentigo, leukoplakia, freckles, melasma, post-inflammatory melanoderma, and moles.[108,111,112] Additionally, the imbalance caused by the ultra violet radiation overthrows intracellular antioxidants and stimulates melanogenesis by upregulating tyrosinase expression and tyrosinase-related proteins 1 and 2.[108,113] In melanin synthesis, the L-tyrosinase enzyme plays a major role in catalyzing the hydroxylation of L-tyrosine to 3,4-dihydroxyphenylalanine and further oxidizes L-DOPA to o-dopaquinone (melanin precursor).[114] Hence, maintaining the adverse effects of the reactive oxygen species at the basal level or preventing tyrosinase action by antityrosinase mixtures could prevent melanin biosynthesis. However, most of the antityrosinase molecules available in the market, such as kojic acid, arbutin, hydroquinone, and corticosteroids, are associated with side effects such as skin irritation, cellular cytotoxicity, contact dermatitis, and reduced enzyme inhibition.[115,116] Thus, there is a need to find a series of natural compounds with enhanced antioxidant and antityrosinase properties that could be used in place of these synthetic compounds. Scn-AgNPs with high antioxidant and antityrosinase inhibition properties could be highly effective and can be further explored for their application in the skin care industry after detailed testing and approval.

Table 2 and Figure 7 show the antibacterial effects of Scn-AgNPs on the three different pathogenic bacteria. The Scn-AgNPs were highly effective against all the three texted pathogen (13.80 mm-16.90 mm dZOIdZOI at 100 µg/disc) (Table 2, Figure 7A). Among the three texted pathogens, the Scn-AgNPs were more effective against *L. monocytogenes* (16.90 mm of inhibition zone). The standard antibiotic, ciprofloxacin (as reference positive control), displayed more effective outcome with the dZOI between 29.8 and 37.10 mm at 10 µg/disc (Table 2, Figure 7B). The MIC and MBC values for Scn-AgNPs on all three tested pathogens ranged from to 25–100 µg/mL and for ciprofloxacin, they ranged from 5.0 to 10.0 µg/mL (Table 2).

The differences in the dZOIs among the tested pathogens could be due to the nature of the mode of action of the nanoparticles and the associated morphological changes in each pathogenic bacterium. Therefore, to study the mode of action of Scn-AgNPs against these pathogens, cell viability, surface morphology, and their effect on salt tolerance of *E. coli* and *E. faecium* were examined (Figure 8). In case of the cell viability test, it is observed that at the MIC concentration of Scn-AgNPs, there was no distinct decline in the viable cell count of *E. coli* until 6 h of incubation, but there was a slight decline in the cell count of *E. faecium* at 6 h of incubation (Figure 8A and B). However, there was a marked decline in the number of cells after 6 h, and the growth completely ceased after 10 h of incubation. In comparison, untreated bacterial cells continued to grow in an increasing order for both pathogens (Figure 8A and B). A possible hypothesis for these trends in the treated pathogens could be associated with the easy penetration of the Scn-AgNPs into bacterial cells because of their smaller size and circular forms, which might result in injury to the cell wall, leading to bacterial leakage and ultimately death of the bacterial cells.[117,118] Similar trends were also observed in the salt

Table 2 Antibacterial Activity of Scn-AgNPs and the Reference Positive Control Against the Pathogenic Bacterial and Their MIC and MBC Values

Pathogens	Scn-AgNPs (at 100 µg/mL)			Ciprofloxacin (at 10 µg/mL)		
	Zone of Inhibition (in mm)*	MIC (in µg/mL)	MBC (in µg/mL)	Zone of Inhibition (in mm)*	MIC (in µg/mL)	MBC (in µg/mL)
Escherichia coli O157:H7,	14.09±0.40^{e}	50	100	28.86±1.01^{c}	5.0	10.0
Enterococcus faecium	13.8±0.36^{e}	50	100	32.04±0.4^{b}	2.5	5.0
Listeria monocytogenes	16.49±0.35^{d}	25	50	36.09±1.1^{a}	2.5	5.0

Notes: *All data are expressed as mean ± standard deviation, and inhibition zones with different superscript letters (a,b,c, d, e) are statistically significant at P<0.05.

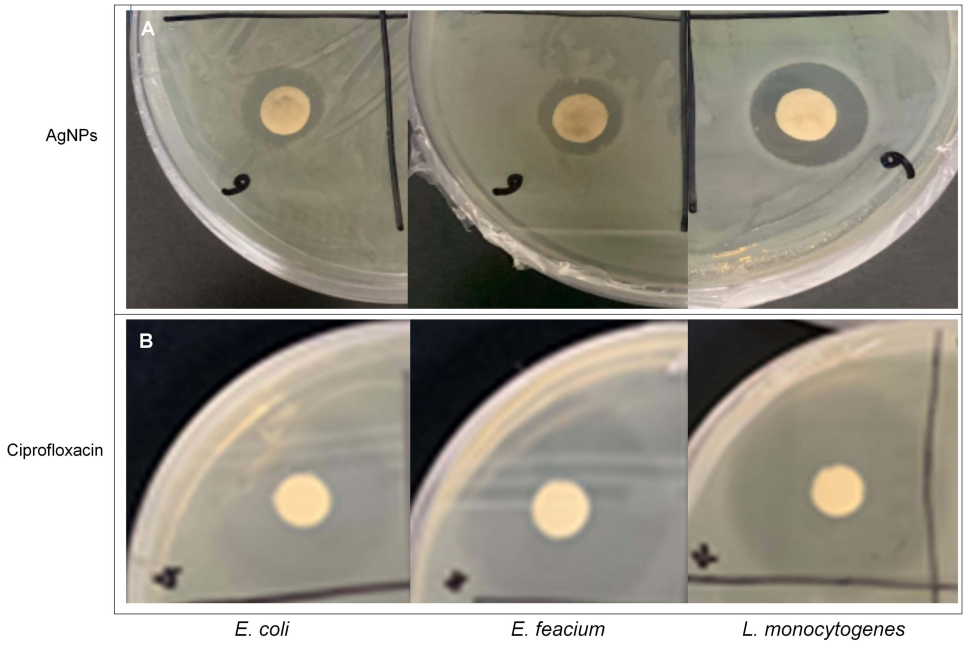

Figure 7 Antibacterial prospective of (**A**) synthesized Scn-AgNPs and (**B**) standard antibiotics-ciprofloxacin against the tested pathogenic bacteria.

tolerant assay, where after the treated and untreated bacteria were plated on NA plates supplemented with altered salt percentages (0%, 2.5%, 5%, and 10%), the treated pathogens showed a some resistance upto 2.5% salt concentration and continued growing (Figure 8C and D). However, there was complete decline in the bacterial growth at 5 and 10% of salt concentrations in both *E. coli* and *E. faecium* as compared to their corresponding control plates, which showed a normal growth at 5% salt concentrations also (Figure 8C and D). The reduction in the capacity of the treated pathogenic bacteria to high salt concentrations indicated that Scn-AgNPs caused severe damage to the bacterial cell membrane and cell surface by the action of Scn-AgNPs.[119] While both *E. coli* and *E. faecium*, treated with the MIC of Scn-AgNPs, were observed for any stress of release of cellular materials, such as nucleic acids, which can be detected at 260 nm in the outer environment, a persistent increase in the quantity of cellular materials was observed at regular incubation times in both the tested bacteria (Figure 8E and F). However, in the control samples without NP treatment, the values remained constant throughout the incubation period (Figure 8E and F). This confirmed that the increase in the amount of intercellular material in the reaction mixture is an indication of leakage in the bacterial cell membrane caused by Scn-AgNP treatment. Finally, based on the results of all three investigations, the conceivable antibacterial mechanism of action of Scn-AgNPs, which can be hypothesized, is that Scn-AgNPs might have attached to the surface of the bacterial cells, causing damage to the outer surface that could have initiated the rupture of the bacterial cell, leading to the discharge of intercellular materials to the outer environment, ultimately leading to cellular lysis and cell death.[120,121] At present, the rise of multidrug-resistant pathogenic microbes in the atmosphere is normal and has resulted in an unfriendly influence on human wellbeing.[122] Considering this, there is an urgent requirement for the development of advanced antibacterial materials that can effectively fight against recently developed multidrug-resistant pathogenic bacteria.[123] Additionally, by using nanoparticles as antibacterial treatment, the scope of gene mutation in the bacterial body is minimized in the nanoparticle-enabled treatment process.[124,125] Additionally, SNPs have been reported to be able to release silver ions constantly, which could affect the bacterial cell walls and might be considered as one of the mechanisms for killing microbes.[126,127] These results indicate that Scn-AgNPs might serve as active antibacterial agents in a number of applications in the biomedical, cosmetic, and food industries.

https://doi.org/10.2147/IJN.S512524

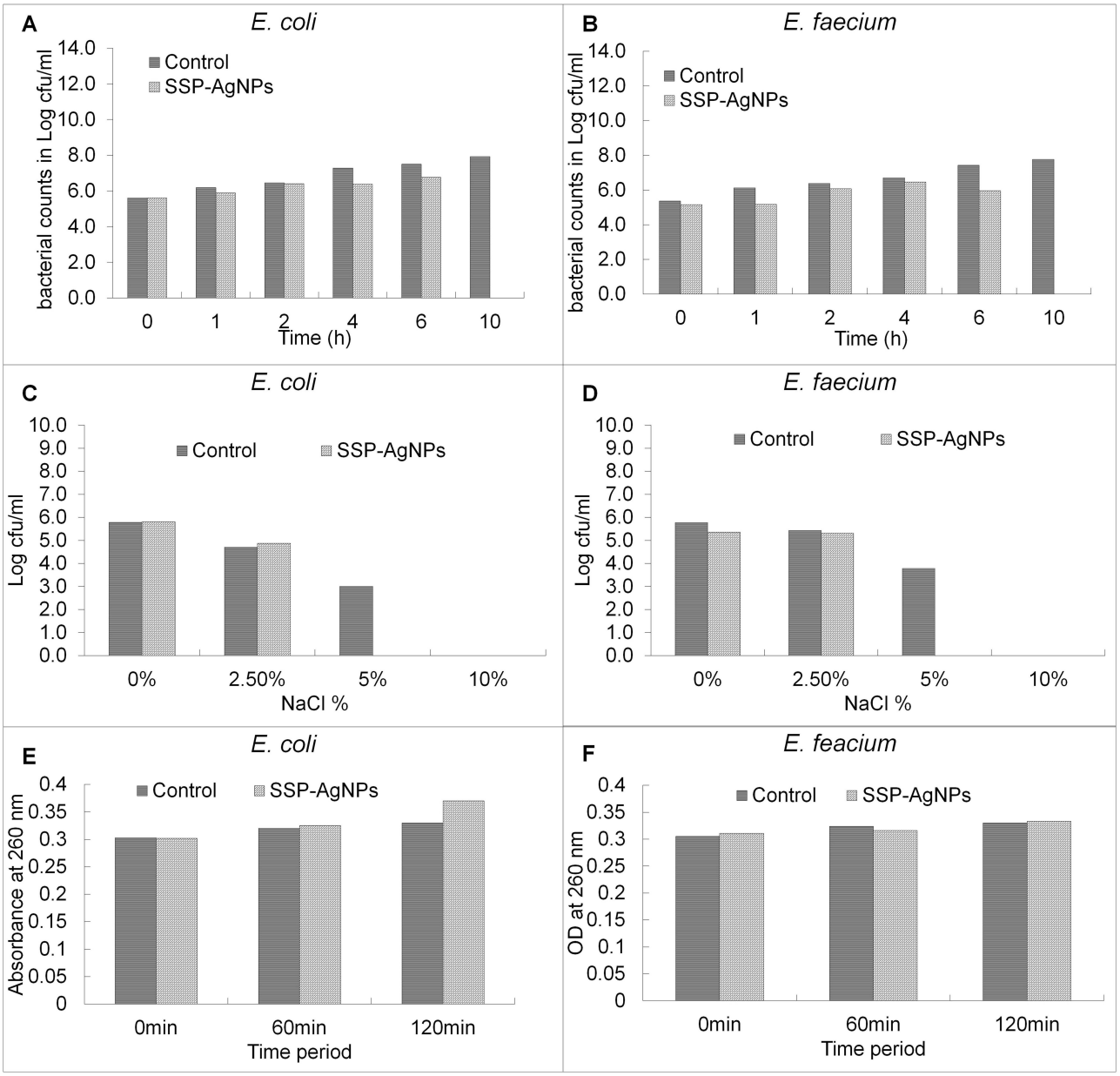

Figure 8 Mechanism of antibacterial action of the synthesized Scn-AgNPs against *E. coli* and *E. faecium*. (**A** and **B**): Cell viability effect; (**C** and **D**): Salt concentration effect; (**E** and **F**): 260 nm absorbing materials effect.

Conclusion

The bio-fabrication of Scn-AgNPs using sericin extract as a capping and stabilizing agent may be a substitute for eco-friendly, cost-effective, and one-pot synthesis techniques for SNPs, which may replace the conventional chemical synthesis approaches. The synthesized Scn-AgNPs were evenly distributed and exhibited a good crystallinity with a mean particle size of 82.77 nm. The Scn-AgNPs demonstrated noteworthy anti-inflammatory properties, promising wound healing, substantial antioxidant, antidiabetic, and tyrosinase inhibition potential, along with significant antibacterial effects. In addition, the possible mode of antibacterial action of Scn-AgNPs was hypothesized to be due to their spherical nature and smaller size, which may have attached to the surface of the bacterial cells, causing damage to the outer surface that could have initiated the rupture of the bacterial cell, leading to the discharge of intercellular materials to the outer environment, which ultimately leads to cellular lysis and cell death. Overall, Scn-AgNPs are advantageous nanoscale-sized candidates for biomedical applications owing to their excellent aqueous stability, in vitro

biocompatibility, and effective anti-inflammatory, antioxidant, antidiabetic, wound healing, and antibacterial properties. More future research needs to be undertaken to formulate commercial products using these Scn-AgNPs for application in cosmetics and food-sector industries.

Acknowledgment

Authors are grateful to Dongguk University, Seoul, South Korea for support. This study was supported by the National Research Foundation of Korea (NRF) grant funded by the Korean government (MSIT) (No. 2020R1G1A1004667), Republic of Korea.

Institutional Review Board Approval

IRB approval is not required for experiments using HaCaT cells (established immortalized cell line).

Funding

This study was supported by the National Research Foundation of Korea (NRF) grant funded by the Korean government (MSIT) (No. 2020R1G1A1004667), Republic of Korea.

Disclosure

Prof. Dr. Jayanta Kumar Patra is serving as an editorial board member of the "*International Journal of Nanomedicine*", but did not participate in the editorial handling and did not have information for the peer-review process of this work. The authors declare that there is no other conflict of interest exists with this manuscript.

References

1. Azarbani F, Shiravand S. Green synthesis of silver nanoparticles by *Ferulago macrocarpa* flowers extract and their antibacterial, antifungal and toxic effects. *Green Chem Lett Rev*. 2020;13(1):41–49. doi:10.1080/17518253.2020.1726504
2. Dhaka A, Mali SC, Sharma S, Trivedi R. A review on biological synthesis of Silver nanoparticles and their potential applications. *Results Chem*. 2023;101108.
3. Raza S, Ansari A, Siddiqui NN, Ibrahim F, Abro MI, Aman A. Biosynthesis of silver nanoparticles for the fabrication of non cytotoxic and antibacterial metallic polymer based nanocomposite system. *Sci Rep*. 2021;11(1):10500. doi:10.1038/s41598-021-90016-w
4. Jiang Z, Li Y, Wei Z, et al. Pressure-induced amorphous zeolitic imidazole frameworks with reduced toxicity and increased tumor accumulation improves therapeutic efficacy In vivo. *Bioact. Mater.* 2021;6(3):740–748. doi:10.1016/j.bioactmat.2020.08.036
5. Zhu L, Bai M, Xiao S, et al. In-situ monitoring of cellular H(2)O(2) within 3D cell clusters using conductive scaffolds. *Talanta*. 2024;279:126559. doi:10.1016/j.talanta.2024.126559
6. Nie Y, Li D, Peng Y, et al. Metal organic framework coated MnO(2) nanosheets delivering doxorubicin and self-activated DNAzyme for chemo-gene combinatorial treatment of cancer. *Int J Pharm*. 2020;585:119513. doi:10.1016/j.ijpharm.2020.119513
7. Rasheed T, Bilal M, Li C, Nabeel F, Khalid M, Iqbal HM. Catalytic potential of bio-synthesized silver nanoparticles using *Convolvulus arvensis* extract for the degradation of environmental pollutants. *J Photochem Photobiol B Biol*. 2018;181:44–52. doi:10.1016/j.jphotobiol.2018.02.024
8. Zhang D, Song J, Jing Z, et al. Stimulus responsive nanocarrier for enhanced antitumor responses against hepatocellular carcinoma. *Int J Nanomed*. 2024;19:13339–13355. doi:10.2147/IJN.S486465
9. Gao Q, Feng J, Liu W, et al. Opportunities and challenges for co-delivery nanomedicines based on combination of phytochemicals with chemotherapeutic drugs in cancer treatment. *Adv Drug Delivery Rev*. 2022;188:114445. doi:10.1016/j.addr.2022.114445
10. Sakellari GI, Zafeiri I, Pawlik A, et al. Independent co-delivery of model actives with different degrees of hydrophilicity from oil-in-water and water-in-oil emulsions stabilised by solid lipid particles via a Pickering mechanism: a-proof-of-principle study. *J Colloid Interface Sci*. 2021;587:644–649. doi:10.1016/j.jcis.2020.11.021
11. Dong Q, Jiang Z. Platinum–iron nanoparticles for oxygen-enhanced sonodynamic tumor cell suppression. *Inorganics*. 2024;12(12):331. doi:10.3390/inorganics12120331
12. Zhang Z, Wang L, Guo Z, Sun Y, Yan J. A pH-sensitive imidazole grafted polymeric micelles nanoplatform based on ROS amplification for ferroptosis-enhanced chemodynamic therapy. *Colloids Surf B*. 2024;237:113871. doi:10.1016/j.colsurfb.2024.113871
13. Wang Y, Xu Y, Song J, et al. Tumor cell-targeting and tumor microenvironment-responsive nanoplatforms for the multimodal imaging-guided photodynamic/photothermal/chemodynamic treatment of cervical cancer. *Int J Nanomed*. 2024;19:5837–5858. doi:10.2147/IJN.S466042
14. Harisha K, Parushuram N, Ranjana R, Martis LJ, Narayana B, Sangappa Y. Characterization and antibacterial properties of biogenic spherical silver nanoparticles. *Mater Today*. 2021;42:405–409.
15. Bordbar M. Biosynthesis of Ag/almond shell nanocomposite as a cost-effective and efficient catalyst for degradation of 4-nitrophenol and organic dyes. *RSC Adv*. 2017;7(1):180–189. doi:10.1039/C6RA24977A
16. Sridhar A, Ponnuchamy M, Kumar PS, Kapoor A. Food preservation techniques and nanotechnology for increased shelf life of fruits, vegetables, beverages and spices: a review. *Environ Chem Lett*. 2021;19:1715–1735. doi:10.1007/s10311-020-01126-2
17. Shivananda CS. Silk fibroin-based green colloidal silver nanoparticle synthesis and their antibacterial and anticancer properties. *Inorg Chem Commun*. 2023;158:111611. doi:10.1016/j.inoche.2023.111611

18. Aramwit P, Bang N, Ratanavaraporn J, Ekgasit S. Green synthesis of silk sericin-capped silver nanoparticles and their potent anti-bacterial activity. *Nanoscale Res Lett*. 2014;9(1):79. doi:10.1186/1556-276X-9-79
19. Sondi I, Goia DV, Matijević E. Preparation of highly concentrated stable dispersions of uniform silver nanoparticles. *J Colloid Interface Sci*. 2003;260(1):75–81. doi:10.1016/S0021-9797(02)00205-9
20. Ali ZA, Yahya R, Sekaran SD, Puteh R. Green synthesis of silver nanoparticles using apple extract and its antibacterial properties. *Adv Mater Sci Eng*. 2016;2016(1):4102196. doi:10.1155/2016/4102196
21. Al Masud M, Shaikh H, Alam M, et al. Green synthesis of silk sericin-embedded silver nanoparticles and their antibacterial application against multidrug-resistant pathogens. *J Genet Eng Biotechnol*. 2021;19(1):1–11. doi:10.1186/s43141-021-00176-5
22. Zhaorigetu S, Yanaka N, Sasaki M, Watanabe H, Kato N. Inhibitory effects of silk protein, sericin on UVB-induced acute damage and tumor promotion by reducing oxidative stress in the skin of hairless mouse. *J Photochem and Photobiol B*. 2003;71(1):11–17. doi:10.1016/S1011-1344(03)00092-7
23. Zhang Y-Q. Applications of natural silk protein sericin in biomaterials. *Biotechnol Adv*. 2002;20(2):91–100. doi:10.1016/S0734-9750(02)00003-4
24. He H, Tao G, Wang Y, et al. In situ green synthesis and characterization of sericin-silver nanoparticle composite with effective antibacterial activity and good biocompatibility. *Mater Sci Eng*. 2017;80:509–516. doi:10.1016/j.msec.2017.06.015
25. Das G, Shin H-S, Campos EVR, et al. Sericin based nanoformulations: a comprehensive review on molecular mechanisms of interaction with organisms to biological applications. *J Nanobiotechnol*. 2021;19(1):1–22. doi:10.1186/s12951-021-00774-y
26. Yang C, Yao L, Zhang L. Silk sericin-based biomaterials shine in food and pharmaceutical industries. *Smart Mater Med*. 2023;4:447–459. doi:10.1016/j.smaim.2023.01.003
27. Laomeephol C, Punjataewakupt A, Kanchanasin P, et al. Silver cross-linking of silk sericin-based hydrogels for improved stability and broad-spectrum antimicrobial properties. *ACS Appl Bio Mater*. 2025;8:2312–2322. doi:10.1021/acsabm.4c01801
28. Arango MC, Yuliet M, Pm S, John B, Álvarez-López C. Silk sericin as a biomaterial for tissue engineering: a review. *Int J Polym Mater Polym Bio mater*. 2021;70(16):1115–1129. doi:10.1080/00914037.2020.1785454
29. Cherng J-H, Chang S-J, Chiu Y-K, Chiu Y-H, Fang T-J, Chen H-C. Low molecular weight sericin enhances the in vitro of immunological modulation and cell migration. *Front Bioeng Biotechnol*. 2022;10:925197. doi:10.3389/fbioe.2022.925197
30. Abirami M, Shayanthi SS, Rajendran R. Synthesis and characterization of PVA based sericin film for antibacterial wound dressing. *Int J Pharm Sci Res*. 2019;10:875–880.
31. Kumar JP, Mandal BB. Silk sericin induced pro-oxidative stress leads to apoptosis in human cancer cells. *Food Chem Toxicolo*. 2019;123:275–287. doi:10.1016/j.fct.2018.10.063
32. Miguel GA, Álvarez-López C. Extraction and antioxidant activity of sericin, a protein from silk. *Braz J Food Technol*. 2020;23. doi:10.1590/1981-6723.05819
33. Tao G, Cai R, Wang Y, et al. Bioinspired design of AgNPs embedded silk sericin-based sponges for efficiently combating bacteria and promoting wound healing. *Mater Des*. 2019;180:107940. doi:10.1016/j.matdes.2019.107940
34. Muhammad Tahir H, Saleem F, Ali S, et al. Synthesis of sericin-conjugated silver nanoparticles and their potential antimicrobial activity. *J Basic Microbiol*. 2020;60(5):458–467. doi:10.1002/jobm.201900567
35. Zhang Y, Zhao Y, He X, et al. A sterile self-assembled sericin hydrogel via a simple two-step process. *Polym Test*. 2019;80:106016. doi:10.1016/j.polymertesting.2019.106016
36. Liu J, Shi L, Deng Y, et al. Silk sericin-based materials for biomedical applications. *Biomaterials*. 2022;287:121638. doi:10.1016/j.biomaterials.2022.121638
37. Qi C, Liu J, Jin Y, et al. Photo-crosslinkable, injectable sericin hydrogel as 3D biomimetic extracellular matrix for minimally invasive repairing cartilage. *Biomaterials*. 2018;163:89–104. doi:10.1016/j.biomaterials.2018.02.016
38. Ai L, Wang Y, Tao G, et al. Polydopamine-based surface modification of Zno nanoparticles on sericin/polyvinyl alcohol composite film for antibacterial application. *Molecules*. 2019;24(3):503. doi:10.3390/molecules24030503
39. Li X, Yang W, Xie H, et al. CNT/sericin conductive nerve guidance conduit promotes functional recovery of transected peripheral nerve injury in a rat model. *ACS Appl Mater Interfaces*. 2020;12(33):36860–36872. doi:10.1021/acsami.0c08457
40. Lamboni L, Xu C, Clasohm J, et al. Silk sericin-enhanced microstructured bacterial cellulose as tissue engineering scaffold towards prospective gut repair. *Mater Sci Eng C*. 2019;102:502–510. doi:10.1016/j.msec.2019.04.043
41. Tao G, Wang Y, Cai R, et al. Design and performance of sericin/poly(vinyl alcohol) hydrogel as a drug delivery carrier for potential wound dressing application. *Mater Sci Eng*. 2019;101:341–351. doi:10.1016/j.msec.2019.03.111
42. Song Y, Zhang C, Zhang J, et al. An injectable silk sericin hydrogel promotes cardiac functional recovery after ischemic myocardial infarction. *Acta Biomater*. 2016;41:210–223. doi:10.1016/j.actbio.2016.05.039
43. Hu D, Xu Z, Hu Z, Hu B, Yang M, Zhu L. pH-triggered charge-reversal silk sericin-based nanoparticles for enhanced cellular uptake and doxorubicin delivery. *ACS Sustainable Chem Eng*. 2017;5(2):1638–1647. doi:10.1021/acssuschemeng.6b02392
44. Dan AK, Aamna B, De S, et al. Sericin nanoparticles: future nanocarrier for target-specific delivery of chemotherapeutic drugs. *J Mol Liq*. 2022;368:120717. doi:10.1016/j.molliq.2022.120717
45. Dhilip Kumar SS, Abrahamse H. Chapter 10 - Sericin-based nanomaterials and their applications in drug delivery. In: Mishra AK, Hussain CM, editors. *Bio-Based Nanomaterials*. Elsevier; 2022:211–229.
46. Summer M, Ali S, Tahir HM, et al. Silk sericin protein: turning discarded biopolymer into ecofriendly and valuable reducing, capping, and stabilizing agent for nanoparticles synthesis using sonication. *Macromol Chem Phys*. 2023;224(17):2300124. doi:10.1002/macp.202300124
47. Shin M, Yang S, Kwak HW, Lee KH. Synthesis of gold nanoparticles using silk sericin as a green reducing and capping agent. *Eur Polym J*. 2022;164:110960. doi:10.1016/j.eurpolymj.2021.110960
48. Shaw S, Mondal R, Dam P, et al. Synthesis, characterization and application of silk sericin-based silver nanocomposites for antibacterial and food coating solutions. *RSC Adv*. 2024;14(45):33068–33079. doi:10.1039/D4RA07056A
49. Teramoto H, Kakazu A, Asakura T. Native structure and degradation pattern of silk sericin studied by 13C NMR spectroscopy. *Macromolecules*. 2006;39(1):6–8. doi:10.1021/ma0521147
50. Mandal S, Selvakannan P, Phadtare S, Pasricha R, Sastry M. Synthesis of a stable gold hydrosol by the reduction of chloroaurate ions by the amino acid, aspartic acid. *J Chem Sci*. 2002;114:513–520. doi:10.1007/BF02704195

51. Das G, Seo S, Yang IJ, Nguyen LTH, Shin HS, Patra JK. Synthesis of biogenic gold nanoparticles by using sericin protein from *Bombyx mori* silk cocoon and investigation of its wound healing, antioxidant, and antibacterial potentials. *Int J Nanomed*. 2023;18:17–34. doi:10.2147/IJN.S378806
52. Das G, Shin HS, Patra JK. Key health benefits of Korean ueong dry root extract combined silver nanoparticles. *Int J Nanomed*. 2022;17:4261–4275. doi:10.2147/IJN.S357343
53. Iravani S, Zolfaghari B. green synthesis of silver nanoparticles using *Pinus eldarica* bark extract. *Biomed Res Int*. 2013;2013:1–5. doi:10.1155/2013/639725
54. Iravani S, Korbekandi H, Mirmohammadi SV, Zolfaghari B. Synthesis of silver nanoparticles: chemical, physical and biological methods. *Res Pharm Sci*. 2014;9(6):385.
55. Das G, Seo S, Yang I-J, Nguyen LTH, Shin H-S, Patra JK. Sericin mediated gold/silver bimetallic nanoparticles and exploration of its multi-therapeutic efficiency and photocatalytic degradation potential. *Environ Res*. 2023;229:115935. doi:10.1016/j.envres.2023.115935
56. Patra JK, Shin H-S, Yang I-J, Nguyen LTH, Das G. Sustainable utilization of food biowaste (papaya peel) extract for gold nanoparticle biosynthesis and investigation of its multi-functional potentials. *Antioxidants*. 2024;13(5):581. doi:10.3390/antiox13050581
57. Patra JK, Das G, Shin H-S. Facile green biosynthesis of silver nanoparticles using *Pisum sativum* L. outer peel aqueous extract and its antidiabetic, cytotoxicity, antioxidant, and antibacterial activity. *Int J Nanomed*. 2019;14:6679–6690. doi:10.2147/IJN.S212614
58. Gowri PM, Tiwari AK, Ali AZ, Rao JM. Inhibition of α-glucosidase and amylase by bartogenic acid isolated from Barringtonia racemosa Roxb. seeds. *Phytother Res*. 2007;21(8):796–799. doi:10.1002/ptr.2176
59. Patra JK, Baek K-H. Antibacterial activity and action mechanism of the essential oil from Enteromorpha linza L. against foodborne pathogenic bacteria. *Molecules*. 2016;21(3):388. doi:10.3390/molecules21030388
60. Harisha K, Shilpa M, Asha S, et al. Synthesis of silver nanoparticles using *Bombyx mori* silk fibroin and antibacterial activity. Paper presented at: IOP Conference Series: Materials Science and Engineering2019.
61. Serrano-Díaz P, Williams DW, Vega-Arreguin J, et al. Geranium leaf-mediated synthesis of silver nanoparticles and their transcriptomic effects on *Candida albicans*. *Green Processing Synthesis*. 2023;12(1):20228105. doi:10.1515/gps-2022-8105
62. Alowaiesh BF, Alhaithloul HAS, Saad AM, Hassanin AA. Green biogenic of silver nanoparticles using polyphenolic extract of olive leaf wastes with focus on their anticancer and antimicrobial activities. *Plants*. 2023;12(6):1410. doi:10.3390/plants12061410
63. Mahakham W, Theerakulpisut P, Maensiri S, Phumying S, Sarmah AK. Environmentally benign synthesis of phytochemicals-capped gold nanoparticles as nanopriming agent for promoting maize seed germination. *Sci Total Environ*. 2016;573:1089–1102. doi:10.1016/j.scitotenv.2016.08.120
64. Ukkund SJ, Raghavendra M, Marigowda YK, Abhinaya N, Puthyillam P. Biosynthesis and characterization of silver nanoparticles from *Penicillium notatum* and their application to improve efficiency of antibiotics Paper presented at: IOP Conference Series: Materials Science and Engineering2019.
65. Tiwari H, Samal K, Geed SR, Bera S, Das C, Mohanty K. Green synthesis of silver nanoparticles for ultrafiltration membrane surface modification and antimicrobial activity. *Sustainable Chem Climate Action*. 2023;3:100031. doi:10.1016/j.scca.2023.100031
66. Arokiyaraj S, Arasu MV, Vincent S, et al. Rapid green synthesis of silver nanoparticles from *Chrysanthemum indicum* L and its antibacterial and cytotoxic effects: an in vitro study. *Int J Nanomed*. 2014;9:379–388. doi:10.2147/IJN.S53546
67. XRDCrystalliteSizeCalculator. XRD Crystallite (grain) Size Calculator (Scherrer Equation) - InstaNANO. Available from: https://instanano.com/all/characterization/xrd/crystallite-size/. Accessed April 28th, 2024.
68. Singh C, Anand SK, Upadhyay R, et al. Green synthesis of silver nanoparticles by root extract of *Premna integrifolia* L. and evaluation of its cytotoxic and antibacterial activity. *Mater Chem Phys*. 2023;297:127413. doi:10.1016/j.matchemphys.2023.127413
69. Saidu FK, Mathew A, Parveen A, Valiyathra V, Thomas GV. Novel green synthesis of silver nanoparticles using clammy cherry (*Cordia obliqua* Willd) fruit extract and investigation on its catalytic and antimicrobial properties. *SN Appl Sci*. 2019;1:1–13. doi:10.1007/s42452-019-1302-x
70. Hamelian M, Varmira K, Veisi H. Green synthesis and characterizations of gold nanoparticles using Thyme and survey cytotoxic effect, antibacterial and antioxidant potential. *J Photochem Photobiol B Biol*. 2018;184:71–79. doi:10.1016/j.jphotobiol.2018.05.016
71. Zhou L, Jiang C, Lin Q. Entropy analysis and grey cluster analysis of multiple indexes of 5 kinds of genuine medicinal materials. *Sci Rep*. 2022;12(1):6618. doi:10.1038/s41598-022-10509-0
72. Pochapski DJ, Carvalho Dos Santos C, Leite GW, Pulcinelli SH, Santilli CV. Zeta potential and colloidal stability predictions for inorganic nanoparticle dispersions: effects of experimental conditions and electrokinetic models on the interpretation of results. *Langmuir*. 2021;37(45):13379–13389. doi:10.1021/acs.langmuir.1c02056
73. Shah A, Ali Buabeid M, Arafa E-SA, Hussain I, Li L, Murtaza G. The wound healing and antibacterial potential of triple-component nanocomposite (chitosan-silver-sericin) films loaded with moxifloxacin. *Int J Pharm*. 2019;564:22–38. doi:10.1016/j.ijpharm.2019.04.046
74. Singh H, Du J, Yi T-H. Green and rapid synthesis of silver nanoparticles using Borago officinalis leaf extract: anticancer and antibacterial activities. *Artif Cells Nanomed Biotechnol*. 2017;45(7):1310–1316. doi:10.1080/21691401.2016.1228663
75. Prema P, Veeramanikandan V, Rameshkumar K, et al. Statistical optimization of silver nanoparticle synthesis by green tea extract and its efficacy on colorimetric detection of mercury from industrial waste water. *Environ Res*. 2022;204:111915. doi:10.1016/j.envres.2021.111915
76. Ali IAM, Ahmed AB, Al-Ahmed HI. Green synthesis and characterization of silver nanoparticles for reducing the damage to sperm parameters in diabetic compared to metformin. *Sci Rep*. 2023;13(1):2256. doi:10.1038/s41598-023-29412-3
77. Chakraborty B, Bhat MP, Basavarajappa DS, et al. Biosynthesis and characterization of polysaccharide-capped silver nanoparticles from *Acalypha indica* L. and evaluation of their biological activities. *Environ Res*. 2023;225:115614. doi:10.1016/j.envres.2023.115614
78. Kalaiyarasu T, Karthi N, Sharmila GV, Manju V. In vitro assessment of antioxidant and antibacterial activity of green synthesized silver nanoparticles from *Digitaria radicosa* leaves. *Asian J Pharm Clin Res*. 2016;9(1).
79. Martínez DCC, Zuluaga CL, Restrepo-Osorio A, Álvarez-López C. Characterization of sericin obtained from cocoons and silk yarns. *Procedia Eng*. 2017;200:377–383. doi:10.1016/j.proeng.2017.07.053
80. Sajanlal PR, Sreeprasad TS, Samal AK, Pradeep T. Anisotropic nanomaterials: structure, growth, assembly, and functions. *Nano Rev*. 2011;2(1):5883.
81. Saha J, Mondal M, Karim Sheikh M, Habib M. Extraction, structural and functional properties of silk sericin biopolymer from *Bombyx mori* silk cocoon waste. *J Text Sci Eng*. 2019;9:2.

82. Moorthy PS. Isolation, purification and characterization of sericin protein from the discharge water of silk industry. *Madras Agricultural Journal*. 2020;107:374–378.
83. Liu Y, Kim S, Kim YJ, et al. Green synthesis of gold nanoparticles using *Euphrasia officinalis* leaf extract to inhibit lipopolysaccharide-induced inflammation through NF-κB and JAK/STAT pathways in RAW 264.7 macrophages. *Int J Nanomed*. 2019;14:2945. doi:10.2147/IJN.S199781
84. Aramwit P, Towiwat P, Srichana T. Anti-inflammatory potential of silk sericin. *Nat Prod Commun*. 2013;8(4):1934578X1300800424. doi:10.1177/1934578X1300800424
85. Choi J-H, Lee S, Han H-J, Kwon J. Antioxidation and anti-inflammatory effects of gamma-irradiated silk sericin and fibroin in H2O2-induced HaCaT Cell. *KorJ Physiol Pharmacol*. 2023;27(1):105–112. doi:10.4196/kjpp.2023.27.1.105
86. Kundu A, Ghosh A, Singh NK, et al. Wound healing activity of the ethanol root extract and polyphenolic rich fraction from *Potentilla fulgens*. *Pharm Biol*. 2016;54(11):2383–2393. doi:10.3109/13880209.2016.1157192
87. Flynn K, Mahmoud NN, Sharifi S, Gould LJ, Mahmoudi M. Chronic wound healing models. *ACS Pharmacol Transl Sci*. 2023;6(5):783–801. doi:10.1021/acsptsci.3c00030
88. Majeed S, Abidin NBZ, Muthukumarasamy R, et al. Wound healing and antidiabetic properties of green synthesized silver nanoparticles in 3T3-L1 mouse embryo fibroblast cells through 2-NBDG expression. *Inorg Chem Commun*. 2024;159:111692. doi:10.1016/j.inoche.2023.111692
89. Nguyen LTH, Ahn S-H, Choi M-J, Yang I-J, Shin H-M. Puerarin improves dexamethasone-impaired wound healing in vitro and in vivo by enhancing keratinocyte proliferation and migration. *Appl Sci*. 2021;11(19):9343. doi:10.3390/app11199343
90. Fang W-C, Lan -C-CE. The epidermal keratinocyte as a therapeutic target for management of diabetic wounds. *Int J Mol Sci*. 2023;24(5):4290. doi:10.3390/ijms24054290
91. Tsubouchi K, Igarashi Y, Takasu Y, Yamada H. Sericin enhances attachment of cultured human skin fibroblasts. *Biosci Biotechnol Biochem*. 2005;69(2):403–405. doi:10.1271/bbb.69.403
92. Micheal A, Subramanyam M. Influence of sericin in alleviating the hydrogen peroxide induced oxidative stress in silkworm *Bombyx mori*: role of the amino acids. *Invertebrate Surv J*. 2014;11(1):257–272.
93. Sangwong G, Sumida M, Sutthikhum V. Antioxidant activity of chemically and enzymatically modified sericin extracted from cocoons of *Bombyx mori*. *Biocatal Agric Biotechnol*. 2016;5:155–161. doi:10.1016/j.bcab.2016.01.010
94. Kumar JP, Mandal BB. Antioxidant potential of mulberry and non-mulberry silk sericin and its implications in biomedicine. *Free Radic Biol Med*. 2017;108:803–818. doi:10.1016/j.freeradbiomed.2017.05.002
95. Lamboni L, Gauthier M, Yang G, Wang Q. Silk sericin: a versatile material for tissue engineering and drug delivery. *Biotechnol Adv*. 2015;33(8):1855–1867. doi:10.1016/j.biotechadv.2015.10.014
96. Takechi T, Wada R, Fukuda T, Harada K, Takamura H. Antioxidant activities of two sericin proteins extracted from cocoon of silkworm (*Bombyx mori*) measured by DPPH, chemiluminescence, ORAC and ESR methods. *Biomed Rep*. 2014;2(3):364–369. doi:10.3892/br.2014.244
97. Dash R, Acharya C, Bindu P, Kundu S. Antioxidant potential of silk protein sericin against hydrogen peroxide-induced oxidative stress in skin fibroblasts. *BMB Reports*. 2008;41(3):236–241. doi:10.5483/BMBRep.2008.41.3.236
98. Demirbas A, Welt BA, Ocsoy I. Biosynthesis of red cabbage extract directed Ag NPs and their effect on the loss of antioxidant activity. *Mater Lett*. 2016;179:20–23. doi:10.1016/j.matlet.2016.05.056
99. Bedlovičová Z, Strapáč I, Baláž M, Salayová A. A brief overview on antioxidant activity determination of silver nanoparticles. *Molecules*. 2020;25(14):3191. doi:10.3390/molecules25143191
100. Al-Radadi NS, Faisal S, Alotaibi A, et al. Zingiber officinale driven bioproduction of ZnO nanoparticles and their anti-inflammatory, anti-diabetic, anti-Alzheimer, anti-oxidant, and anti-microbial applications. *Inorg Chem Commun*. 2022;140:109274. doi:10.1016/j.inoche.2022.109274
101. Rizwana H, Aljowaie RM, Al Otibi F, et al. Antimicrobial and antioxidant potential of the silver nanoparticles synthesized using aqueous extracts of coconut meat (*Cocos nucifera* L). *Sci Rep*. 2023;13(1):16270. doi:10.1038/s41598-023-43384-4
102. Podsedek A, Majewska I, Redzynia M, Sosnowska D, Koziołkiewicz M. In vitro inhibitory effect on digestive enzymes and antioxidant potential of commonly consumed fruits. *J Agr Food Chem*. 2014;62(20):4610–4617. doi:10.1021/jf5008264
103. Rokkarukala S, Cherian T, Ragavendran C, et al. One-pot green synthesis of gold nanoparticles using *Sarcophyton crassocaule*, a marine soft coral: assessing biological potentialities of antibacterial, antioxidant, anti-diabetic and catalytic degradation of toxic organic pollutants. *Heliyon*. 2023;9(3):e14668. doi:10.1016/j.heliyon.2023.e14668
104. Ullah S, Shah SWA, Qureshi MT, et al. Antidiabetic and hypolipidemic potential of green AgNPs against diabetic mice. *ACS Appl Bio Mater*. 2021;4(4):3433–3442. doi:10.1021/acsabm.1c00005
105. Dong X, Zhao S-X, Yin X-L, Wang H-Y, Wei Z-G, Zhang Y-Q. Silk sericin has significantly hypoglycaemic effect in type 2 diabetic mice via anti-oxidation and anti-inflammation. *Int J Biol Macromol*. 2020;150:1061–1071. doi:10.1016/j.ijbiomac.2019.10.111
106. Wang HD, Zhong ZH, Weng YJ, Wei ZZ, Zhang YQ. Degraded sericin significantly regulates blood glucose levels and improves impaired liver function in T2D rats by reducing oxidative stress. *Biomolecules*. 2021;11(8):1255. doi:10.3390/biom11081255
107. Kato N, Sato S, Yamanaka A, Yamada H, Fuwa N, Nomura M. Silk protein, sericin, inhibits lipid peroxidation and tyrosinase activity. *Biosci Biotechnol Biochem*. 1998;62(1):145–147. doi:10.1271/bbb.62.145
108. Kumar JP, Mandal BB. The inhibitory effect of silk sericin against ultraviolet-induced melanogenesis and its potential use in cosmeceutics as an anti-hyperpigmentation compound. *Photochem Photobiol Sci*. 2019;18(10):2497–2508. doi:10.1039/c9pp00059c
109. Cherdchom S, Sereemaspun A, Aramwit P. Urea-extracted sericin is potentially better than kojic acid in the inhibition of melanogenesis through increased reactive oxygen species generation. *J Tradit Complement Med*. 2021;11(6):570–580. doi:10.1016/j.jtcme.2021.06.005
110. Lin JY, Fisher DE. Melanocyte biology and skin pigmentation. *Nature*. 2007;445:7130):843–850. doi:10.1038/nature05660
111. Briganti S, Camera E, Picardo M. Chemical and instrumental approaches to treat hyperpigmentation. *Pigment Cell Res*. 2003;16(2):101–110. doi:10.1034/j.1600-0749.2003.00029.x
112. Han E, Chang B, Kim D, Cho H, Kim S. Melanogenesis inhibitory effect of aerial part of *Pueraria thunbergiana* in vitro and in vivo. *Arch Dermatol Res*. 2015;307:57–72. doi:10.1007/s00403-014-1489-z
113. Alam MB, Bajpai VK, Lee J, et al. Inhibition of melanogenesis by jineol from *Scolopendra subspinipes* mutilans via MAP-Kinase mediated MITF downregulation and the proteasomal degradation of tyrosinase. *Sci Rep*. 2017;7(1):45858. doi:10.1038/srep45858

114. Parvez S, Kang M, Chung HS, et al. Survey and mechanism of skin depigmenting and lightening agents. *Phytother Res*. 2006;20(11):921–934. doi:10.1002/ptr.1954
115. García-Gavín J, González-Vilas D, Fernández-Redondo V, Toribio J. Pigmented contact dermatitis due to kojic acid. A paradoxical side effect of a skin lightener. *Contact Dermatitis*. 2010;62(1):63–64. doi:10.1111/j.1600-0536.2009.01673.x
116. Jones K, Hughes J, Hong M, Jia Q, Orndorff S. Modulation of melanogenesis by aloesin: a competitive inhibitor of tyrosinase. *Pigment Cell Res*. 2002;15(5):335–340. doi:10.1034/j.1600-0749.2002.02014.x
117. Rai A, Prabhune A, Perry CC. Antibiotic mediated synthesis of gold nanoparticles with potent antimicrobial activity and their application in antimicrobial coatings. *J Mater Chem*. 2010;20(32):6789–6798. doi:10.1039/c0jm00817f
118. Sikkema J, de Bont JA, Poolman B. Interactions of cyclic hydrocarbons with biological membranes. *J Biol Chem*. 1994;269(11):8022–8028. doi:10.1016/S0021-9258(17)37154-5
119. Jenie BSL, Priosoeryanto BP, Syarief R, Rekso GT, Rekso GT. Mode of action Temu kunci (*Kaempferia pandurata*) essential oil on E. coli K1. 1 cell determined by leakage of material cell and salt tolerance assays. *HAYATI J Biosci*. 2008;15(2):56–60. doi:10.4308/hjb.15.2.56
120. Kota S, Dumpala P, Anantha RK, Verma MK, Kandepu S. Evaluation of therapeutic potential of the silver/silver chloride nanoparticles synthesized with the aqueous leaf extract of *Rumex acetosa*. *Sci Rep*. 2017;7(1):1–11. doi:10.1038/s41598-017-11853-2
121. Das G, Patra JK. Evaluation of antibacterial mechanism of action, tyrosinase inhibition, and photocatalytic degradation potential of sericin-based gold nanoparticles. *Int J Mol Sci*. 2023;24(11):9477. doi:10.3390/ijms24119477
122. Pugazhendhi A, Kumar SS, Manikandan M, Saravanan M. Photocatalytic properties and antimicrobial efficacy of Fe doped CuO nanoparticles against the pathogenic bacteria and fungi. *Microb Pathogenesis*. 2018;122:84–89. doi:10.1016/j.micpath.2018.06.016
123. Coelho N, Jacinto JP, Silva R, Soares JC, Pereira AS, Tavares P. Green synthesis and antibacterial activity of silver nanoparticles obtained from *Moringa oleifera* seed cake. *Coatings*. 2023;13(8):1439. doi:10.3390/coatings13081439
124. Ahmad S, Ahmad S, Xu Q, et al. Green synthesis of gold and silver nanoparticles using crude extract of *Aconitum violaceum* and evaluation of their antibacterial, antioxidant and photocatalytic activities. *Front Bioeng Biotechnol*. 2024;11:1320739. doi:10.3389/fbioe.2023.1320739
125. Chandraker SK, Kumar R. Biogenic biocompatible silver nanoparticles: a promising antibacterial agent. *Biotechnol Genet Eng Rev*. 2022;40;1–35.
126. Ramkumar VS, Pugazhendhi A, Gopalakrishnan K, et al. Biofabrication and characterization of silver nanoparticles using aqueous extract of seaweed *Enteromorpha compressa* and its biomedical properties. *Biotechnol Rep*. 2017;14:1–7. doi:10.1016/j.btre.2017.02.001
127. Yin Z IX, J ZIS, Mei ML, Li Q, Chu CH. The antibacterial mechanism of silver nanoparticles and its application in dentistry. *Int j Nanomed*. 2020:2555–2562.